MARTIN MARIETTA ENERGY SYSTEMS LIBRARIES

3 4456 0374291 1

ORNL/TM-12274

OAK RIDGE NATIONAL LABORATORY

MARTIN MARIETTA

THERMAL RESPONSE OF GATOR SYSTEM INTERNAL COMPONENTS

John C. Moyers
Kenneth W. Childs
Therese K. Stovall

April 15, 1993

OAK RIDGE NATIONAL LABORATORY
CENTRAL RESEARCH LIBRARY
CIRCULATION SECTION
4500N ROOM 175
LIBRARY LOAN COPY
DO NOT TRANSFER TO ANOTHER PERSON
If you wish someone else to see this report, send in name with report and the library will arrange a loan.

MANAGED BY
MARTIN MARIETTA ENERGY SYSTEMS, INC.
FOR THE UNITED STATES
DEPARTMENT OF ENERGY

This report was prepared as an account of work sponsored by an agency of the United States Government. Neither the United States Government nor any agency thereof, nor any of their employees, makes any warranty, express or implied, or assumes any legal liability or responsibility for the accuracy, completeness, or usefulness of any information, apparatus, product, or process disclosed, or represents that its use would not infringe privately owned rights. Reference herein to any specific commercial product, process, or service by trade name, trademark, manufacturer, or otherwise, does not necessarily constitute or imply its endorsement, recommendation, or favoring by the United States Government or any agency thereof. The views and opinions of authors expressed herein do not necessarily state or reflect those of the United States Government or any agency thereof.

ORNL/TM-12274

THERMAL RESPONSE OF GATOR SYSTEM INTERNAL COMPONENTS

John C. Moyers
Kenneth W. Childs
Therese K. Stovall

April 15, 1993

Prepared for the
Product Assurance Directorate
U.S. Army Armament Munitions
and Chemical Command under Interagency Agreement
1892A078A1

Prepared by the
OAK RIDGE NATIONAL LABORATORY
Oak Ridge, Tennessee 37831-8045
managed by
MARTIN MARIETTA ENERGY SYSTEMS, INC.
for the
U.S. DEPARTMENT OF ENERGY
under contract DE-AC05-84OR21400

MARTIN MARIETTA ENERGY SYSTEMS LIBRARIES

3 4456 0374291 1

TABLE OF CONTENTS

ABSTRACT 1

1. INTRODUCTION 1

2. SYSTEM DESCRIPTION 2
   2.1 The BLU-91/B Antitank Mine 2
   2.2 The CBU-89/B Dispenser-Mine Assembly 3

2.3 Operational Sequence 7

3. AMBIENT AND EFFECTIVE EXPOSURE TEMPERATURES 8
   3.1 Ambient Temperatures 8
   3.2 Effective Exposure Temperatures 8
   3.3 Weapons in Bomb Bay 12

4. ANALYSIS APPROACH 13
   4.1 Computer Models 13
   4.2 Hand Calculations 17

5. ANALYSIS RESULTS 20
   5.1 Computer Models 20
   5.2 Hand Calculations 24

6. MISSION APPLICATIONS 28
   6.1 Mission Temperature Profile 28
   6.2 Applying Normalized Step Temperature Data 28

7. CONCLUSIONS 33

REFERENCES 34

LIST OF FIGURES

Figure 1. Schematic of BLU-91/B Antitank Mine. 2
Figure 2. Air Force Gator CBU-89/B. 3
Figure 3. Air Force Gator Cross-Section, Forward and Rear Sections. 5
Figure 4. Air Force Gator Cross-Section, Center Portion. 5
Figure 5. Minimum Temperatures over North America in January (95% confidence level). 9
Figure 6. Minimum Temperatures over North America in January (99% confidence level). 9
Figure 7. Model 1 two-dimensional finite difference grid. 15
Figure 8. Model 3 two-dimensional finite element grid. 16
Figure 9. Results from finite difference analysis of Model 1 for varying external heat transfer coefficients. 20
Figure 10. Results from finite difference analysis of Model 2 for three angular positions of mine in Row H. 21
Figure 11. Results from finite element analysis of Model 3 with low-conductivity polyurethane for three mine locations. 22
Figure 12. Results from finite element anlysis of Model 3 with high-conductivity polyurethane for three mine locations. 23
Figure 13. Model 3 results for low-conductivity (0.0145 Btu/h-ft-°F) polyurethane applied to mission with 60°F initial and -40°F recovery temperatures. 24
Figure 14. Model 3 results for high-conductivity (0.0242 Btu/h-ft-°F) polyurethane applied to mission with 60°F initial and -40°F recovery temperatures. 25
Figure 15. Results from finite element anlysis for Row H mine in Model 3 with low-conductivity polyurethane for three external heat transfer coefficients. 25
Figure 16. Results from finite element analysis of Row H in Model 3 with high-conductivity polyurethane for three external heat transfer coefficients. 26
Figure 17. Comparison of Model 2 (HEATING 7) and Model 3 (TOPAZ) results for Row H mine during a mission with 60°F initial and -40°F recovery temperatures. 27
Figure 18. Effects of ambient temperaure, Mach number, and recovery factor on recovery temperature. 29
Figure 19. Predicted external exposure duration at which internal mine temperature drops to -25°F, based on results from Model 2 30
Figure 20. Predicted bomb bay exposure duration at which internal mine temperature drops to -25°F, based on results from Model 2. 31

ABSTRACT

The Gator Weapon System may be subjected to severe temperature extremes. One internal component of this system is known to be sensitive to very low temperatures. An analysis of the system was therefore made to determine the relationship between the environmental temperatures and the Gator's internal temperature profile. These internal temperature projections can then be used to define the external conditions under which the system would be prone to failure. Three detailed computer models and one simplified model were used to explore the thermal response of the Gator to a step environmental temperature change. The response to this nondimensionalized step change can then be used to predict the internal Gator temperatures for a variety of mission profiles. The study was also therefore able to determine if there was a possibility that the Gator would encounter the necessary external conditions required to bring about the cold temperature failure scenario. The results show the Gator mines to be well protected with a relatively slow thermal response. For example, given an initial temperature of 15.6°C (60°F) and a recovery temperature of -40°C (-40°F) [this recovery temperature is the result of a speed of Mach 0.77, recovery factor of 0.89, and ambient temperature of -62.2°C (-80°F)], the critical component temperature drops to the limiting value of -31.7°C (-25°F) only after exposure times greater than 12 hours.

---

1. INTRODUCTION

The Gator Weapon System provides the means for air delivery and emplacement of a mine field that consists of a mix of antipersonnel and antiarmor mines. The mines are packed into dispensers that are delivered to the application area suspended from either external or internal racks of the delivery aircraft. Thus, the weapons are exposed, depending upon mission and delivery aircraft, to a wide range of ambient temperatures.

Each mine contains electronic circuitry that provides, among other functions, a timing feature that causes the mine to self-destruct after a preset time interval following emplacement, thereby clearing the mine field before the planned arrival of friendly ground forces. One component, a capacitor in the antitank mine circuitry, has demonstrated a tendency to fail upon exposure to extreme cold, thereby disrupting the timing function and resulting in mines with unpredictable self-destruct behavior. Specifically, after repeated thermal cycles between +71.1 and -51.1°C (+160 and -60°F), a capacitor in the timing circuit of the mine electronics assembly occasionally shorts during cooldown through approximately -31.7°C (-25°F), resulting in an erratic timing function.

The U.S. Army Armament Munitions and Chemical Command, at Picatinny Arsenal, which has programmatic responsibility for the mines, requested that Oak Ridge National Laboratory perform thermal modeling of the Gator System to provide estimates of mine internal temperature as a function of initial and at-altitude temperatures and mission duration. This report presents a description of the Gator system, the modeling methodology, and the results obtained.

2. SYSTEM DESCRIPTION

Two versions of the Gator system, one for the U.S. Air Force and the other for the U.S. Navy, are used. The Air Force version, designated CBU-89/B, utilizes a dispenser that contains 22 antipersonnel mines and 72 antitank mines. The Navy version, designated CBU-78/B, is smaller and contains 15 antipersonnel mines and 45 antitank mines. The mines used in both versions are of the same type, with BLU-92/B antipersonnel mines and BLU-91/B antitank mines utilized. Because the Air Force missions tend to be at higher altitude and of longer duration, the following description applies to, and the modeling effort concentrated on, this version. Furthermore, since the cold-exposure problem has only been encountered in the antitank mine, the mine description is limited to the BLU-91/B.

2.1 The BLU-91/B Antitank Mine

The BLU-91/B antitank mine is shown schematically in Fig. 1. The mine is contained in its mild steel case and stainless steel cover plates. Two steel plates, shaped like spherical segments lie against the top and bottom of the shaped main charge, which consists of 0.6 kg (1.3 lb) of cyclotrimethylenetrinitramine (RDX) explosive. A small booster charge, located in the center hole of the main charge and surrounding the safe and arming (S&A) assembly, amplifies the initiating impulse from the S&A assembly and sets off the main charge. This S&A assembly is constructed mainly of zinc. The electronic lens, of cast epoxy, contains the electronic circuit board with its associated battery, with the circuit board lying just inside the flat base of the lens. A magnetic coupling coil located on the base of the lens picks up signals from an adjacent coil on a strip line from the dispenser central electronics module to start mine activation and establish time to self-destruct.

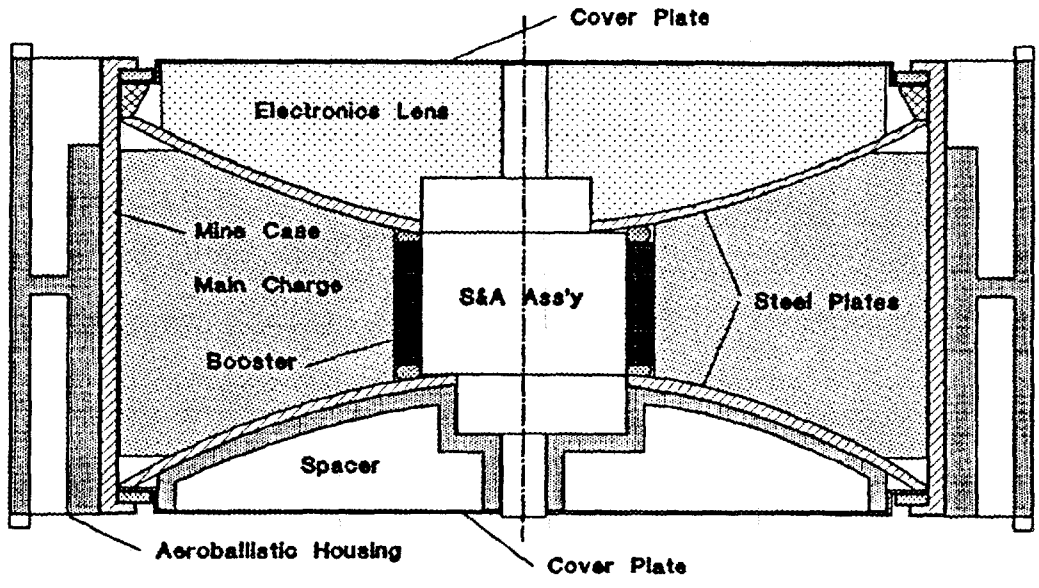

Figure 1. Schematic of BLU-91/B Antitank Mine.

The basic steel-cased mine geometry is that of a 12.1 cm (4.75 in.) diameter by 6.6 cm (2.6 in.) long cylinder. The mine is cemented into a rectangular aeroballistic housing, cast of acrylonitrile-butadiene-styrene (ABS) plastic, that causes the mine-housing assembly to rotate around a transverse axis during free-fall. Outside dimensions of the housing are 12.7 by 14.6 by 7.0 cm (5 by 5.75 by 2.76 in.) high. Total assembly weight is 2.0 kg (4.3 lb). The dimensions of the antipersonnel mine and the antitank mine are identical, permitting packing the mix of the two types into a uniform array in the dispenser, but the antipersonnel mine weighs only 1.7 kg (3.7 lb).

Each mine has a spring-loaded borerider pin that protrudes through the cover plate on the spacer end of the mine. The mine is assured in the safe condition so long as the end of the pin is maintained nearly flush with the outside surface of the cover plate, as when the mines are packed in the dispenser. The mine electronics circuitry is powered by two lithium batteries that have extended shelf life because their electrolyte is stored in a glass ampule until the mine is released from the dispenser.

2.2 The CBU-89/B Dispenser-Mine Assembly

A longitudinal view of the CBU-89/B dispenser-mine assembly, as used by the Air Force, is shown in Fig. 2. The dispenser in which the mines are packed consists of a cylindrical body with a rounded nose section containing the mechanical time fuze and optional proximity sensor and a tail section containing the electronics assembly that provides signals to individual mines via the stripline harness. Antispin fins, folded during storage and aircraft delivery but spring-loaded to deploy after leaving the aircraft, are mounted on the tail section.

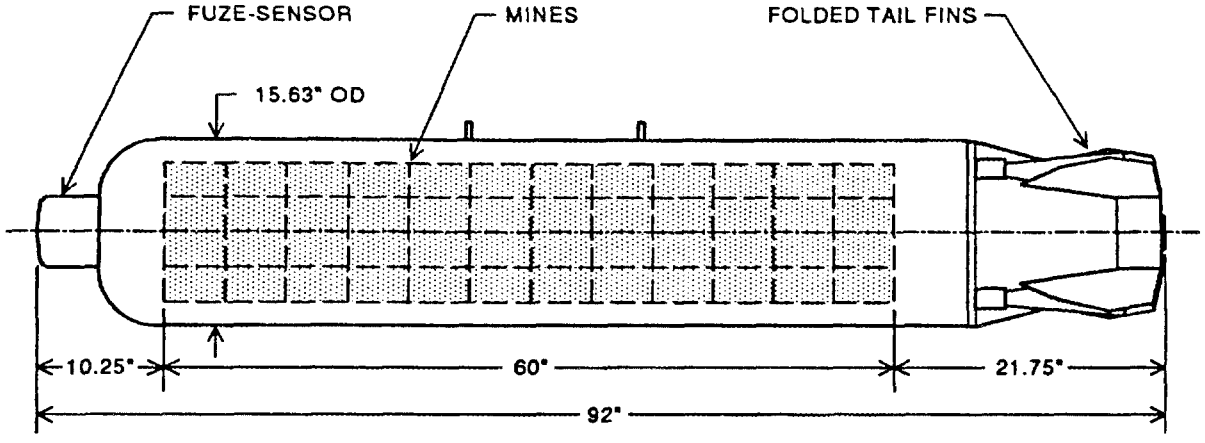

Figure 2. Air Force Gator CBU-89/B.

Three full-length linear shaped charges are installed against the inside surface of the dispenser to open the dispenser at a selected time interval after the dispenser separates from the aircraft (mechanical fuze) or at a selected altitude (proximity sensor/fuze) and allow the mines to free-fall individually to the ground.

The electronics assembly is powered by a thermal battery that charges a capacitor bank to provide a strong burst of power to the stripline harness to accomplish the transfer of self-destruct timing information to the individual mines.

A cross-section, applicable to the forward and rear portions of the dispenser-mine assembly, is shown in Fig. 3. The mines are packed in seven rows of 12 mines each and one row of 10 mines, with the thermal battery located in the two empty spaces located at the rear of the short row. Dunnage blocks of polyurethane foam (items 1 - 6 and item 12 in the figure) fill the spaces between the cylindrical dispenser shell and the rectangular rows of mines. The dunnage insures that the mines fit snugly in the dispenser, but also functions as thermal insulation between the mines and the aluminum dispenser shell. Two filler strips of fiberboard (items 8 and 9) and one of aluminum (item 7) complete the packing. The shaped cutting charges fit in the three open channels in the dunnage. The eight striplines that deliver the self-destruct timing signals to the mines lie along the right face (as oriented in the figure) of the mine rows.

In the midlength portion of the assembly, for a length of 91 cm (36 in.), the top dunnage block is replaced by an extruded aluminum strongback as shown in Fig. 4. The strongback (item 10) serves to reinforce the aluminum dispenser shell and distributes the load from the suspension shackle lugs to the shell. The materials shown in Figs. 3 and 4 are summarized in Table 1.

Table 1. Gator cross-section materials shown in Figs. 3 and 4.

No.	Description	Material
1	Packing, Upper Right	Polyurethane Foam
2	Packing, Right Side	Polyurethane Foam
3	Packing, Lower Right	Polyurethane Foam
4	Packing, Lower Left	Polyurethane Foam
5	Packing, Left Side	Polyurethane Foam
6	Packing, Upper Left	Polyurethane Foam
7	Strip, Spacer, 0.17 cm (1/16 in.) thick	6061 Aluminum Alloy
8	Strip, Spacer, 0.33 cm (1/8 in.) thick	Hardboard
9	Strip, Spacer, 0.66 cm (1/4 in.) thick	Hardboard
10	Strongback	6061 Aluminum Alloy
11	Skin, Body Section	Aluminum (assumed)
12	Packing, Upper Forward and Rear	Polyurethane Foam

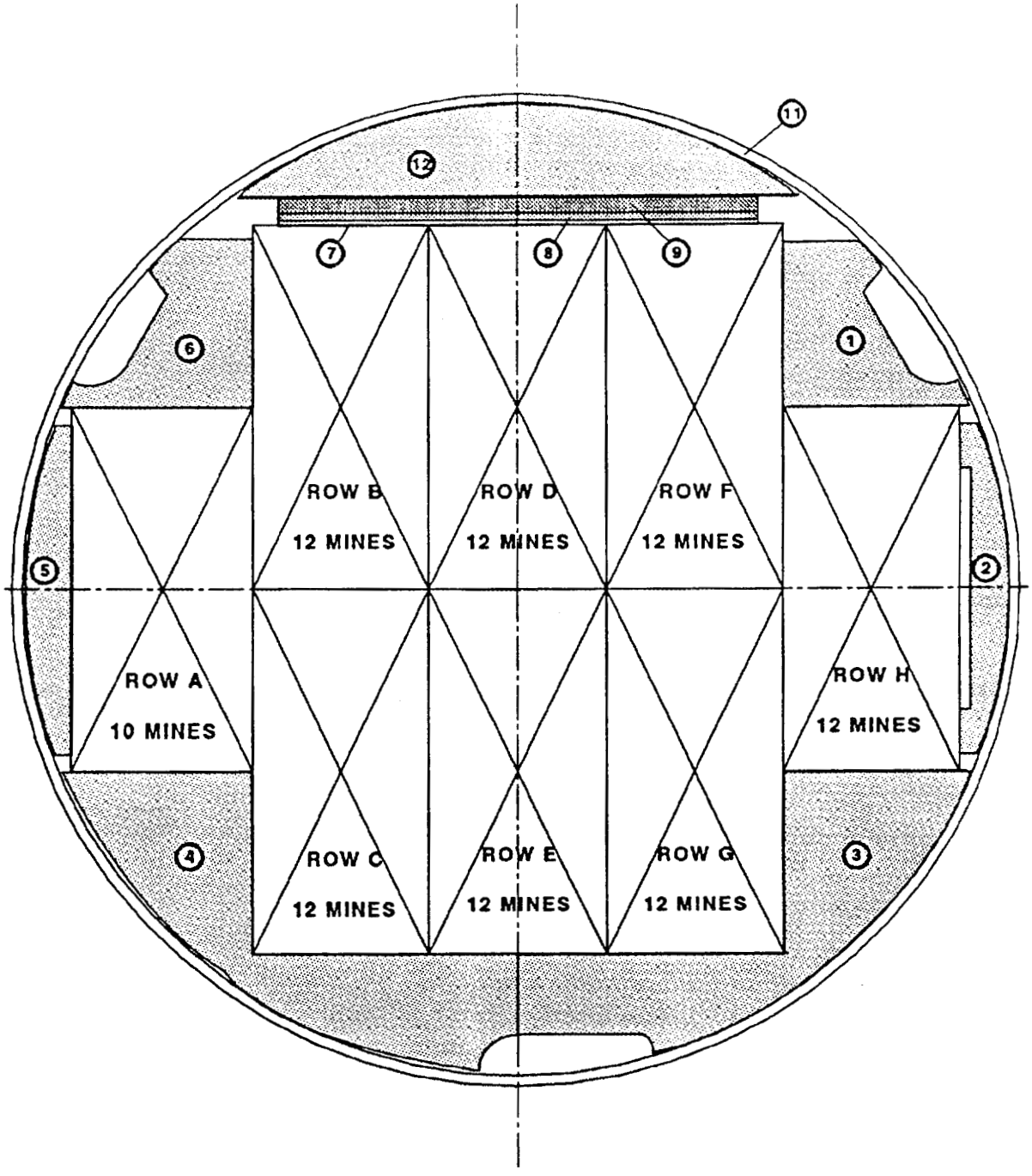

Figure 3. Air Force Gator Cross-Section, Forward and Rear Sections.

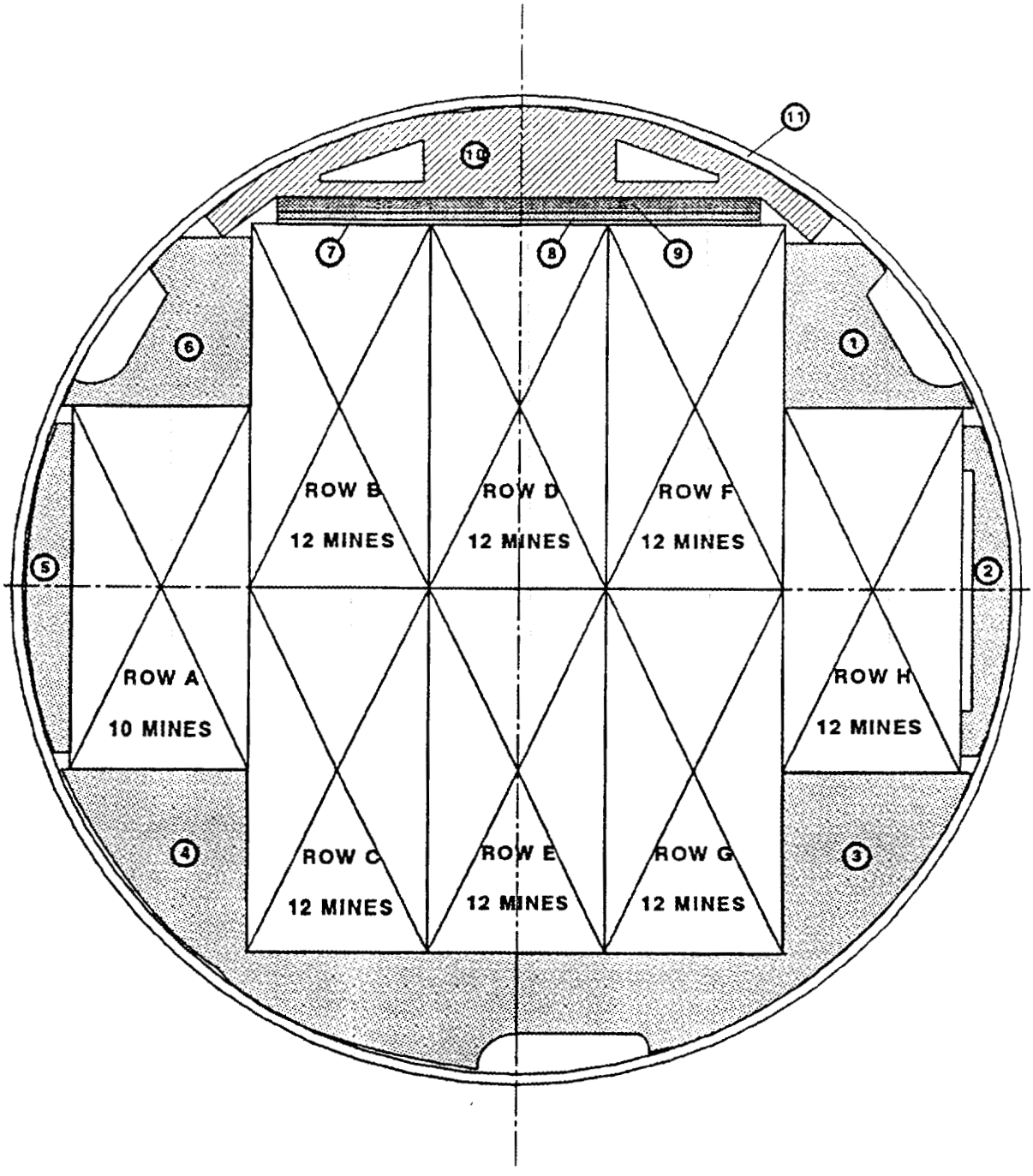

Figure 4. Air Force Gator Cross-Section, Center Portion.

2.3 Operational Sequence

As the Gator weapon is loaded on the delivery aircraft, the self-destruct time is manually selected by means of a switch on the dispenser. Two lanyards, one to activate the fuze and the other to open the folded tail fins, are attached to the aircraft bomb rack. Later, as the weapon is released over the target area, the lanyards are extracted from the dispenser and remain with the aircraft.

Extraction of the lanyards opens the spring-loaded tail fins and activates the thermal battery. The thermal battery quickly builds to its full output level and charges the capacitor packs that will later power the dispenser electronics package to provide the mine activation and self-destruct time signals to the individual mines.

At the preselected time (mechanical fuze) or altitude (proximity sensor-fuze), the linear shaped charges fire to open the dispenser. The shock from the shaped charges also closes an event switch, which releases the capacitor pack energy through the dispenser electronics package and sends the signals down the striplines to the mines. The mine batteries are activated when the electrolyte ampules are shattered upon receipt of the stripline signal, starting an internal clock.

When the dispenser opens and the mines disperse in free-fall, the boreriders are released and the mine's safe and arming sequence begins. As the mines fall and disperse in a random pattern, their aeroballistic housings cause them to spin about a transverse axis to stabilize their flight and help them come to rest in an upright position.

The mine arming sequence is completed after two minutes of elapsed time on the clock, after the mine has come to rest on the ground. The antipersonnel mines then deploy triplines that will set off the mine if disturbed. The antitank mines align themselves electronically with the earth's magnetic field and will detonate if the magnetic field is disturbed by movement or by proximity of an approaching steel mass. If not activated by a target or disturbance, the mines will self-destruct at the preset time. The mines will also self-destruct when the mine battery is exhausted.

3. AMBIENT AND EFFECTIVE EXPOSURE TEMPERATURES

The Gator mine/dispenser assembly may be delivered to the intended target area by either tactical or strategic aircraft. Delivery by strategic aircraft is deemed to pose the most severe exposure to extreme cold, due to long-duration missions at high altitude. When carried by the B-52 strategic bomber, Gators may be hung from external bomb racks under the aircraft wing and from internal racks in the bomb bay. Nominal cruising velocity and altitude of this aircraft are taken to be 226 m/s and 10.7 km (440 knots and 35,000 ft.).

3.1 Ambient Temperatures

Temperature extremes at various altitudes are presented in MIL-STD-210C.[1] Low temperature extremes at an altitude of 10 km (32,800 ft) and having frequencies of occurrence of 1, 5, 10, and 20% are -74, -72, -70, and -65°C (-101, -98, -94, and -85°F), respectively. These values apply to the most severe month in the worst part of the world. As such, they are not representative of temperatures that would be encountered in most missions and, if encountered, exposure would be of short duration. For example, traversing 10 degrees of latitude in a north-south direction takes approximately 1.4 hours at B-52 cruising velocity.

The limitations of using MIL-STD-210C extreme temperatures are recognized by Appendix A of MIL-STD-1670A,[2] which recommends using the *U.S. Standard Atmosphere, 1962*, or its 1966 supplement. The newer 1976 revision[3] provides temperatures at altitude that are "roughly representative of year-round, midlatitude conditions." The temperature given for an altitude of 10 km (32,800 ft) is -50°C (-58°F), with systematically variable monthly mean temperatures at any location between the equator and the pole ranging approximately between -61 and -36.7°C (-78 and -34°F).

A more definitive characterization of temperatures at various altitudes and latitudes is provided by the *Handbook of Geophysics and Space Environments*.[4] Monthly mean temperatures over North America at altitude and latitudes between -7 and 27°C (20 and 80°F), along with standard deviations to account for seasonal changes around the monthly mean and diurnal variability, are presented for January and July. Minimum January temperatures for altitudes of 9,144; 12,190; and 15,240 m (30,000; 40,000; and 50,000 ft.), at 95% and 99% confidence levels as determined by deducting two or three standard deviations (assuming normal distribution), respectively, from the mean value are plotted in Figs. 5 and 6.

3.2 Effective Exposure Temperatures

The effective exposure temperature that provides the driving potential for heat loss from the weapon during captive flight is denoted as the 'recovery' temperature. The recovery temperature is warmer than the ambient temperature because of aerodynamic heating resulting from conversion of the kinetic energy of the passing air stream to thermal energy. If complete kinetic energy conversion is achieved, as at the front of a blunt body, the resulting temperature is the 'stagnation' temperature which is calculable by the following relationship.

$$T^o = T\left(1 + \frac{\gamma - 1}{2} M^2\right) \tag{1}$$

where:

T^o = stagnation temperature, absolute,
T = ambient temperature, absolute,

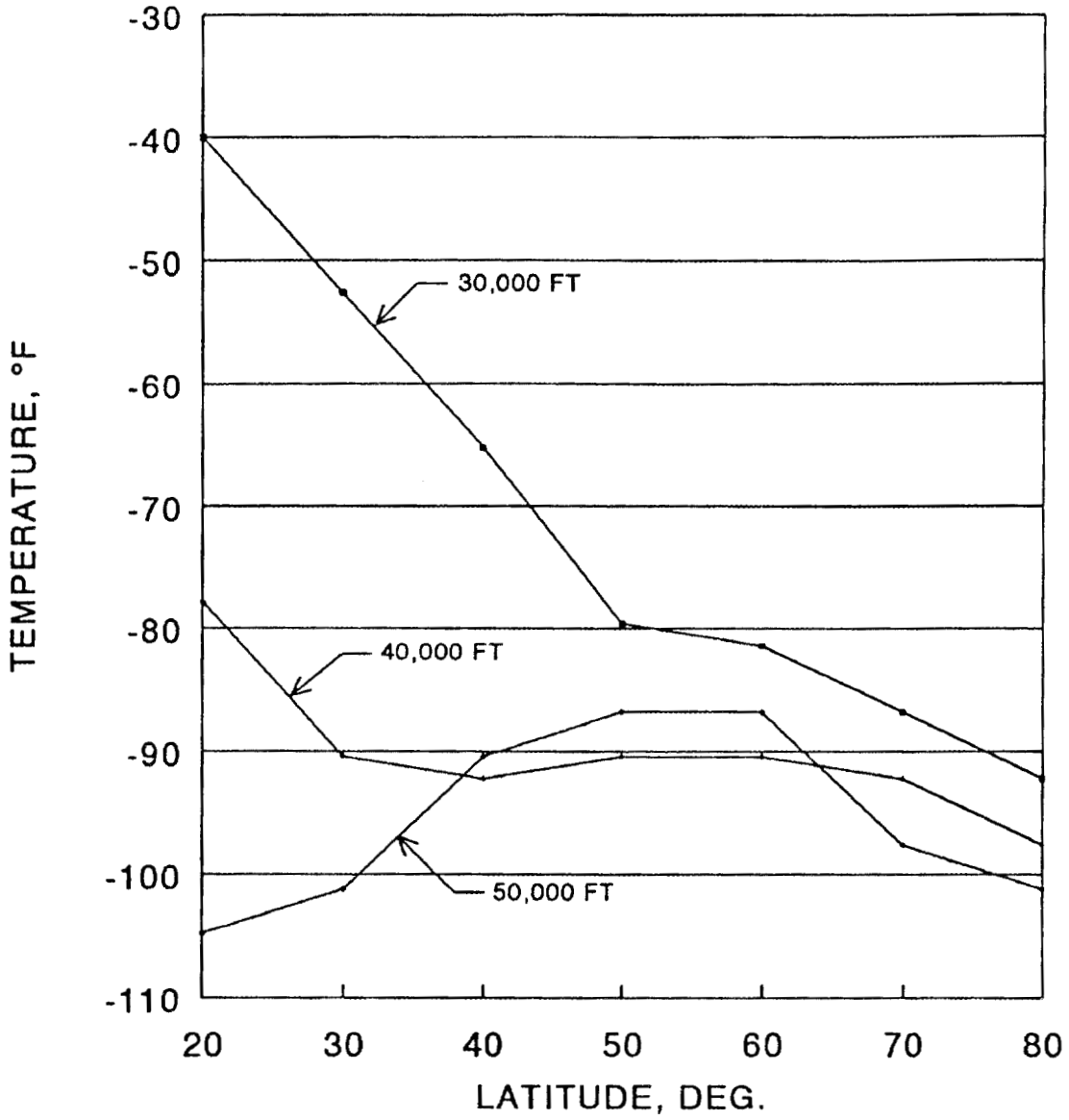

Figure 5. Minimum Temperatures over North America in January (95% confidence level).

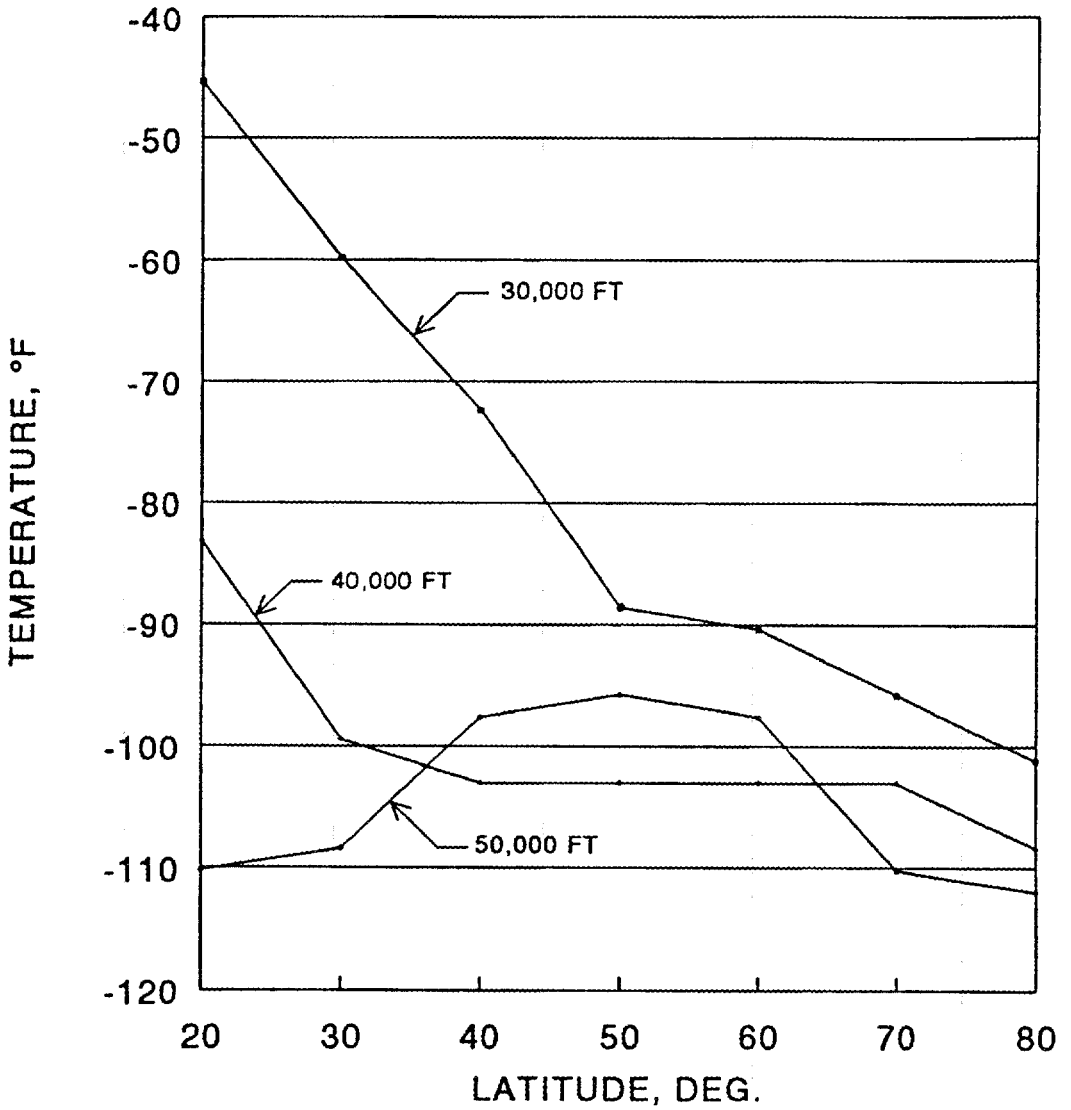

Figure 6. Minimum Temperatures over North America in January (99% confidence level).

γ = specific heat ratio for air, and
M = Mach number.

Using a value of 1.4 (typical for air) for γ yields

$$T^o = T(1 + 0.2M^2) \tag{2}$$

In actuality, complete conversion of the kinetic energy is not realized and the recovery temperature is somewhat cooler than the stagnation temperature. This effect is recognized by the introduction of the recovery factor, r, into the above relationship to calculate recovery temperature as follows.

$$T_r = T(1 + 0.2rM^2) \tag{3}$$

where:

T_r = recovery temperature, absolute and
r = recovery factor.

McAdams[5] and others evaluate recovery factor for flow parallel to a flat plate to be equal to the square root of Prandtl number for laminar flow and approximately equal to the cube root of Prandtl number for turbulent flow. The Prandtl number at the altitude of interest is approximately 0.74, yielding recovery factors of 0.86 for laminar flow and 0.90 for turbulent flow.

In a Navy report[6] covering flight tests in which Navy Quickstrike Mark 65 mines were carried both in the bomb bay and under the wing of a B-52, data are presented that permit back-calculating recovery factors for those mines. [The critical limiting minimum temperature for these mines is -40°C (-40°F)]. From one of the test flights, a recovery factor of 0.805 resulted while, for another flight, the resulting recovery factor was only 0.548. The cause of the difference between the two flights is not known, but it is not believed to be from different installation locations under the wing. The Navy conclusions include the following statement.

> "There was little difference noted in the data for different locations of the mines on the wing, and it is felt that there will be essentially no difference of temperature with mine location on the wing of the B-52."

In Appendix A of MIL-STD-1670A,[2] the following relationships are given for calculating recovery temperature.

For laminar flow (Reynolds number <500,000 when evaluated using distance from leading edge as the characteristic dimension):

$$T_r = T(1 + 0.170M^2) \tag{4}$$

For turbulent flow (Reynolds number > 500,000):

$$T_r = T(1 + 0.178M^2) \tag{5}$$

The implied recovery factors used to develop these two equations, for laminar and turbulent flow, are 0.85 and 0.89.

These various values for recovery factor and the recovery temperatures that result from each when the ambient temperature is -62°C (-80°F) and the aircraft Mach number is 0.77 are summarized in Table 2. Except for the one anomalous point from the second Navy flight, the variations of recovery temperature resulting from differences in recovery factor are minor and the numbers recommended by MIL-STD-1670A were used for the remainder of the work on this project.

Table 2. Example recovery factors and temperatures

Recovery factor source	Laminar		Turbulent	
	r	t_r,°C (°F)	r	t_r,°C (°F)
Prandtl number	0.86	-41 (-41)	0.90	-39 (-39)
Navy flight 1			0.805	-42 (-44)
Navy flight 2			0.548	-48 (-55)
MIL-STD-1670A	0.85	-41 (-42)	0.89	-40 (-40)

3.3 Weapons in Bomb Bay

The weapons carried in the bomb bay are exposed to environmental conditions that are markedly different than for those carried under the wing. The convective film coefficient is much less, essentially limited to that for natural convection. The outside skin temperature of the B-52 should be approximately the recovery temperature as shown in Sect. 3.2. In view of this and the contribution of heat from internal plane systems to the bomb bay volume, bomb bay temperatures should be much greater than the ambient temperatures.

Two points of reference for bomb bay temperature were identified. Mr. Dean Cunningham, of Tinker Air Force Base, stated that bomb bay temperatures in the B-52 rarely are below -23°C (-10°F). The Navy report[6] states that, during the two instrumented flights when the lowest outside air temperature was -53 and -49°C (-63 and -56°F), the measured temperature of the weapon in the bomb bay never went below -12°C (+10°F) and concluded that:

> "Based on this, it is obvious that no limitations nor restrictions need be placed on bomb bay carriage of the Quickstrike Mark 65 mine in the B-52."

4. ANALYSIS APPROACH

The Gator can be subjected to a wide range of mission conditions, as described in Sect. 3. Therefore, the analysis was performed in a manner that would allow the results to be used to predict Gator temperatures under a wide range of environmental profiles.

4.1 Computer Models

The complex construction of the Gator mine and dispenser clearly indicated the need for a detailed computer model. The accuracy of the model's results depends on the size and arrangement of the grid used for numerical calculations and on the numerical method selected. These same factors determine the amount of programming effort and computer resources needed for the analysis. Therefore, this analysis was accomplished in a series of three steps to provide the necessary information with a reasonable degree of effort. All component properties used in the computer models are shown in Table 3. All of these properties were assumed constant (i.e., not a function of temperature), and a conservative value was chosen whenever the literature provided a range of values. Two polyurethane foam materials were examined because the conductivity of the Gator dunnage was not known, although the density was specified to be 3.3 lb/ft^3. The dunnage conductivity will be affected by the manufacturing process parameters, including the foaming agent, curing temperature, and curing time. The two dunnage materials examined here are reasonably expected to bracket the likely conductivity of the Gator materials. The uncertainty associated with this issue is addressed in Sect. 5.

Table 3. Material properties for computer models

Material	Conductivity (Btu/h-ft-°F)	Density (lb/ft^3)	Specific Heat (Btu/lb-°F)
RDX	0.168	114.2	0.30
Booster	0.168	114.2	0.30
Carbon Steel	42.66	490.8	0.15
304 Stainless Steel	7.45	484.4	0.12
Epoxy	0.109	74.9	0.25
Zinc	65.10	445.8	0.092
Aluminum	72.62	168.6	0.20
ABS	0.121	64.9	0.36
Hardboard	12.0	62.5	0.32
Polyurethane Foam 1	0.0145	2.50	0.40
Polyurethane Foam 2	0.0242	3.75	0.40

All analyses were based on a step temperature change with the Gator system assumed to be at a known uniform temperature at the start of the mission. The step temperature change can be described in two ways. In its simplest form, it represents a temperature change of one degree in the environment. The results can then be interpreted to show how quickly the mine responds to this environmental change and approaches the new environmental temperature. The step temperature change can also be represented as a dimensionless, normalized temperature (which also varies from 0 to 1). The dimensionless temperature is actually the ratio of two temperature differences as shown in Eq. 6.

$$T_n = \frac{T_t - T_i}{T_\infty - T_i} \tag{6}$$

where:

T_n	=	dimensionless, normalized temperature of mine,
T_t	=	temperature within the mine at time t after occurrence of step change,
T_i	=	initial temperature of Gator and environment, and
T_∞	=	environmental temperature at all times after step change.

Model 1

The first step was to analyze the worst-case temperature exposure of the antitank mine circuitry. A simplified model was defined and examined for this worst case to determine whether or not more detailed models were required. This first analysis of a Gator mine utilized a two-dimensional R-Z (axisymmetric) model. This approximation envisions a mine with no variations in the rotational direction, so that a single plane can represent the entire 360° of the cylindrical shape. Since there is an approximate plane of symmetry at the midplane of the mine, only the lower half of the mine (i.e., the half containing the electronics lens) was modeled. All internal components were modeled as solid objects. The hole through the zinc casting and the cavities in the epoxy lens were not modeled. The only cavity in the model is adjacent to the outer circumference of the lens. This cavity was conservatively assumed to present a resistance to heat flow of 0.18 m^2-°C/W (1.0 h-ft^2-°F/Btu). All adjacent internal components were assumed to be in perfect thermal contact with each other (i.e., no contact resistance, another conservative assumption). Since the electronics lens is modeled as a solid block of epoxy, the circuit board and electronic components were not explicitly modeled. The plastic aeroballistic housing was not included in this model.

The finite-difference heat transfer code, HEATING 7.1, was used to perform the analyses.[7] The limitations of this computer program required that several minor geometric approximations be made in the model. The shape of the curved stainless steel plates separating the main charge from the electronic lens was approximated as a stair-step configuration, and the asymmetric zinc casting was modeled as axisymmetric. The resulting finite-difference mesh used in the analyses is shown in Fig. 7. Four different cases were run with this model. In each of these cases the mine was subjected to a step change in the environmental temperature but with different external heat transfer coefficients ranging from 5.68 W/m^2-°C (1 Btu/h-ft^2-°F) to infinity (a step change in surface temperature). All external surfaces of the mine were exposed to these conditions in the model. A value of 5.68 W/m^2-°C (1 Btu/h-ft^2-°F) approximates natural convection. High speed air flow over the mine would produce a heat transfer coefficient somewhere in the range of 57 to 142 W/m^2-°C (10 to 25 Btu/h-ft^2-°F). The results of these analyses are discussed in Sect. 5. They showed that the mine would respond very quickly to any temperature change at the mine's surface. Therefore, more detailed modeling of the Gator system was required.

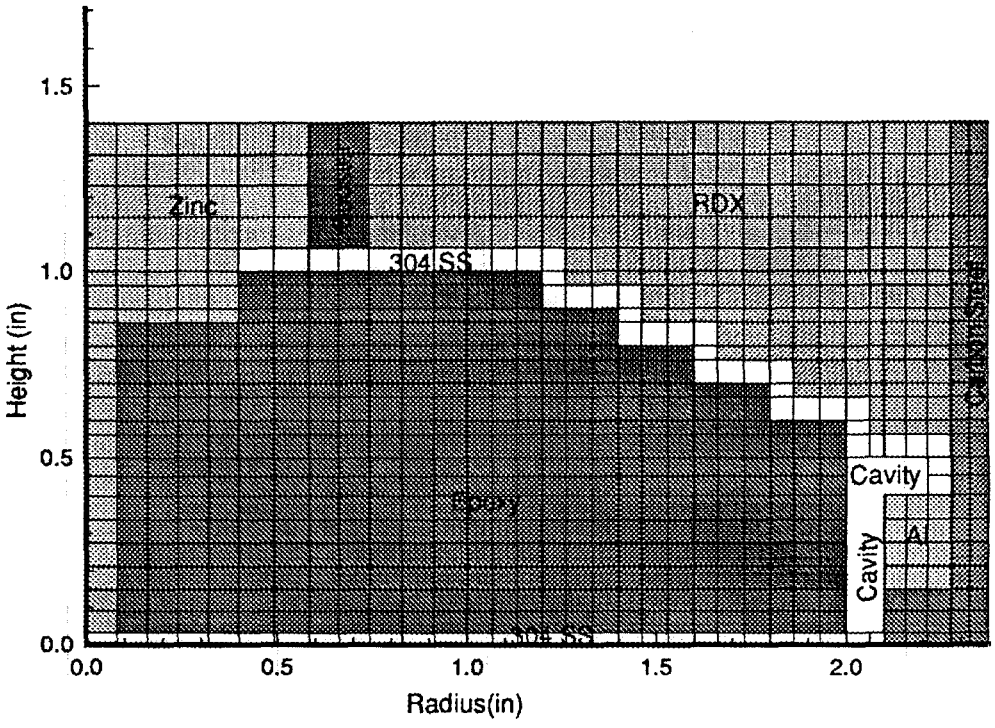

Figure 7. Model 1 two-dimensional finite difference grid.

Model 2

The results from the analyses of Model 1 indicated that the thermal protection provided by the dispenser housing will largely determine if the failure-prone capacitor will drop to unacceptably low temperatures. Mines in Rows A and H are nearest the surface of the dispenser and thus might be expected to cool more rapidly than mines in the other rows (later work showed the temperature exposure of these rows and those near the aluminum strongback to be very nearly the same). Therefore Model 1 was extended to approximate the condition of a mine in Row H, where the mine orientation places the electronic lens closest to the dispenser surface. The mesh of Model 1 was rotated through a 90° angle to produce a three-dimensional pie-shaped sector of a mine. A portion of the ABS aerodynamic housing consisting of the 0.28 cm (0.11 in.)-thick ring in direct contact with the mine was also included in the model. The remainder of the aeroballistic housing, the polyurethane dunnage, and the dispenser housing were not explicitly included in the finite-difference model, but, rather, were included as an effective heat transfer coefficient on the surface of the model. The complex shape of the aeroballistic housing and the interconnected air cavities within and around the aeroballistic housing, and the uncertainties in the heat transfer mechanisms between the aeroballistic housing and the dispenser housing made a detailed model impractical at this stage of the project. Therefore the resistance to heat transfer from the surface of the mine assembly, including the ABS ring, to the inner surface of the polyurethane dunnage was assigned a value of 0.18 m^2-°C/W (1 h-ft^2-°F/Btu). In all likelihood, this resistance will be higher, but this value represents a limiting case. Added to this resistance value is a resistance representing conduction through the polyurethane dunnage (this resistance is position dependent since the thickness varies), the resistance

of the aluminum housing (negligible for practical purposes), and the resistance associated with the external heat transfer coefficient. For this calculation the polyurethane density was assumed to be 40 kg/m^3 (2.5 lb/ft^3) and the corresponding thermal conductivity from the HEATING 7.1 properties table was used. Cutouts in the polyurethane dunnage were neglected in calculating the resistance (i.e., they were assumed to be polyurethane filled). The surface heat transfer coefficient on the exterior of the missile was assumed to be 56.8 W/m^2-°C (10 Btu/h-ft^2-°F) which corresponds to a resistance of 0.02 m^2-°C/W (0.1 h-ft^2-°F/Btu). This model was also analyzed using HEATING 7.1. When the cylindrical mine is placed inside the rectangular aerodynamic housing, the rotational position of the mine is variable. Therefore, the analysis examined three mine rotational positions representing 0°, 45°, and 90° azimuthal positions of the failure-prone capacitor. The 0° position corresponds to the mine being rotated so that the capacitor is located below the minimum polyurethane dunnage thickness. The 90° position corresponds to the mine rotation necessary to place the capacitor beneath the maximum polyurethane dunnage thickness, with the 45° position representing a midway location. Results of the analysis, discussed in detail in Sect. 5, showed that the mine remains fairly uniform in temperature throughout the transient. This uniformity indicates that the detailed model of the mine itself was not necessary because the temperature of the electric circuitry is controlled not by the mine construction, but by the other Gator components.

Model 3

Since the previous work showed that the thermal response of the mines is controlled by heat flow through components external to the mines, including the assembly housing and the polyurethane dunnage,

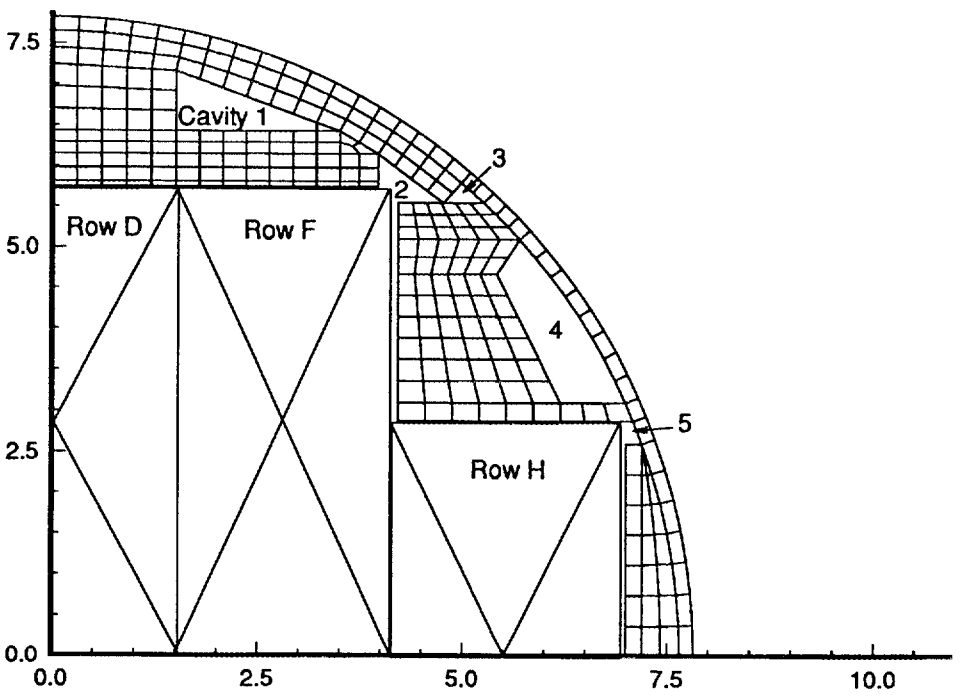

Figure 8. Model 3 two-dimensional finite element grid.

a more detailed model of these components was needed. The effect of the increased heat transfer through the aluminum strongback was also unknown. Therefore, a finite-element computer program, TOPAZ 2D, was used to model the complex shape of the assembly housing, strongback, and dunnage.[8] That model is shown in Fig. 8. Since very little temperature variation is expected within a mine, each of the mines was modeled as a single lumped-capacitance node. As in Model 2, the contact resistance to heat flow between the mines and the surrounding dunnage and assembly housing was assumed to be 0.18 m^2-°C/W (1 h-ft^2-°F/Btu). There are five air cavities in the model which are identified by number in Fig. 8. Cavities 1 and 4 are large relative to the others and may develop natural circulation loops. These cavities were modeled with a bulk fluid temperature and a heat transfer coefficient of 5.68 W/m^2-°C (1 Btu/h-ft^2-°F) between the air and the cavity walls. Cavities 2 and 5 are too small to sustain significant convection but do permit heat transfer directly from the mines to the aluminum assembly housing. In these cavities, heat transfer was also modeled by a surface-to-surface heat transfer coefficient of 5.68 W/m^2-°C (1 Btu/h-ft^2-°F) between the mine surface and the housing inner surface. No heat transfer was modeled in Cavity 3 since it does not significantly affect the heat transfer to the mines. The elements above Rows D and F, surrounding Cavity 1, represent the aluminum strongback and hardboard and aluminum fillers, as can be seen more clearly in Fig. 4 (items 7-10). The elements beside Rows F and H represent the polyurethane dunnage. As in Model 2, the external surface heat transfer coefficient was set to 56.8 W/m^2-°C (10 Btu/h-ft^2-°F). The sensitivity of the results to both polyurethane density and external heat transfer coefficient variations was also examined.

4.2 Hand Calculations

As described in the previous section, the complexities of the Gator system necessitate a detailed model to accurately predict the heat transfer paths and the resulting internal temperature profiles. It is prudent, however, to corroborate these results using a simpler analytic technique, if possible. Towards that end, the dynamic response of a simple, homogenous cylinder was examined to provide a rough estimate of the internal temperature profiles. These approximate results should be accurate enough to provide an order of magnitude verification of the computer analysis.

The internal temperature profile of a long homogenous cylinder exposed to a step change in the environmental temperature can be calculated using Eqs. 7 and 8.[9]

$$T_n^* = \left(\frac{T_t - T_\infty}{T_i - T_\infty}\right) = 2 \sum_{n=1}^{\infty} \frac{Bi\, e^{-\mu_n^2 Fo} J_0(\mu_n \rho)}{(\mu_n^2 + Bi^2) J_0(\mu_n)} \tag{7}$$

$$\mu_n J_1(\mu_n) - Bi\, J_0(\mu_n) = 0 \tag{8}$$

where:

- T_n^* = nondimensionalized temperature within infinitely long cylinder at radial position r,
- T_t = temperature within infinitely long cylinder at radial position r and time t,
- T_i = initial temperature of cylinder and environment,
- T_∞ = environmental temperature at all times after step change,
- R = cylinder radius,
- μ_n = root found from Eq. 8,
- J_0, J_1 = Bessel functions,

ρ = r/R,
Fo = Fourier number ($\alpha t/R^2$), and
Bi = Biot number (hR/k).

This nondimensionalized temperature is equal to one minus the nondimensionalized temperature used for all the computer modeling efforts and shown in Eq. 6. Both are shown in Sect. 5 to make comparisons between the two analyses easier.

Due to the complex structure of the Gator mines, three conductivities were examined for the assumed homogeneous composite. The lowest conductivity reflects the component with the lowest conductivity, the ABS aerodynamic housing. Within the structure, these housing pieces are in direct contact with each other and could form an effective barrier to heat transfer. However, the steel casings around the explosive component provide relatively quicker heat transfer along the length of each mine. A mass-averaged conductivity was chosen to represent the upper bound of the internal conductivity, reflecting the effect of the casing's higher conductivity while still including some correction for the resistance offered by the other components. A third estimate uses the volume fractions of the various components to weight the conductivity according to the Eucken equation for a two-component mixture where one component is considered continuous and the other noncontinuous.[10]

$$K_m = K_1 \frac{1 - f + f\,[3K_2/(2K_1 + K_2)]}{1 - f + f\,[3K_1/(2K_1 + K_2)]} \tag{9}$$

where: K_m = volume-average conductivity,
K_1 = conductivity of continuous phase,
K_2 = conductivity of noncontinuous phase, and
f = volume fraction of noncontinuous phase.

This equation only represents two components and was therefore applied twice in series to determine an overall Gator conductivity. First, the mine itself was modeled as a continuous steel shell [k=45.8 W/m-°C (26.5 Btu/h-ft-°F)] with a discontinuous RDX/epoxy/zinc component [k=2.9 W/m-°C (1.7 Btu/h-ft-°F)]. This produced a volume averaged mine conductivity of 11.6 W/m-°C (6.7 Btu/h-ft-°F). The Eucken equation was then applied to a continuous structure of ABS [k=0.17 W/m-°C (0.1 Btu/h-ft-°F)] with a discontinuous mine component. This produced a volume-weighted internal Gator conductivity of 1.6 W/m-°C (0.94 Btu/h-ft-°F). This volume-weighted value is likely to be a better predictor (compared to the lowest and mass-averaged conductivities) of the heat flow through the various Gator components because the volume fractions would better reflect the cross sectional areas available for heat transfer. These values are all shown in Table 4.

The insulating effects of the polyurethane dunnage were modeled by including them in an effective external convective heat transfer coefficient. Insulating values for polyurethane cover a broad range. The value used for this portion of the analysis was 0.028 W/m-°C (0.016 Btu/h-ft-°F). The external film coefficient was assumed to be relatively high, 56.8 W/m^2-°C (10 Btu/h-ft^2-°F). The minimum dunnage thickness near the mines was about 0.66 cm (0.26 in.). Using the appropriate relationship for heat transfer in series in a cylindrical configuration, and assuming a constant insulation thickness of 0.66 cm (0.26 in.), the effective heat transfer coefficient is 4.42 W/m^2-°C (0.778 Btu/h-ft^2-°F).

In another section of the Gator, the polyurethane dunnage is displaced by an aluminum stiffener with a hardboard layer between the aluminum and the mines. This section could offer much better heat transfer than the other portions of the missile. It was therefore modeled using the same external convective coefficient of 56.8 W/m^2-°C (10 Btu/h-ft^2-°F), an aluminum conductivity of 202 W/m-°C

(117 Btu/h-ft-°F) (higher than that used for the computer models) and the minimum strongback thickness of 1.6 cm (0.069 ft), and a hardboard conductivity of 0.143 W/m-°C (0.083 Btu/h-ft-°F) and thickness of 10.2 cm (0.031 ft). Arranged in series in a radial configuration as before, this gives an effective external heat transfer coefficient of 11.2 W/m^2-°C (1.98 Btu/h-ft^2-°F).

Table 4. Component properties for hand calculations[11,12,13]

Material	Conductivity [W/m-°C (Btu/h-ft-°F)]	Density [kg/m^3(lb/ft^3)]	Specific Heat [kJ/kg-°C (Btu/lb-°F)]	Thermal Diffusivity [m^2/s(ft^2/h)]
steel	45.8 (26.5)	7,820 (488)	0.46 (0.11)	
RDX	0.29 (0.168)	1,760 (110)	1.3 (0.3)	
epoxy	0.87 (0.5)	1,120 (70)	1.05 (0.25)	
zinc	112. (65.0)	7,140 (446)	0.4 (0.09)	
ABS	0.17 (0.1)	1,040 (65)	1.5 (0.35)	
Composite (mass-average conductivity)	27.3 (15.8)	1,510 (94)	0.84 (0.20)	2.2E-5 (0.84)
Composite (lowest conductivity)	0.17 (0.1)	1,510 (94)	0.84 (0.20)	1.4E-7 (.0053)
Composite (Eucken conductivity)	1.63 (0.94)	1,510 (94)	0.84 (0.20)	1.3E-6 (0.05)

5. ANALYSIS RESULTS

5.1 Computer Models

The results of the initial computer model described in Sect. 4.1 are presented in Fig. 9 as temperature-vs-time plots at the location of the electronic circuitry of concern. These results indicated that the capacitor temperature would very rapidly drop to unacceptable levels [< -31.7°C (-25°F)] if the mine were to be directly exposed to the external, in-flight conditions represented by an external heat transfer coefficient of about 56.8 W/m²-°C (10 Btu/h-ft²-°F).

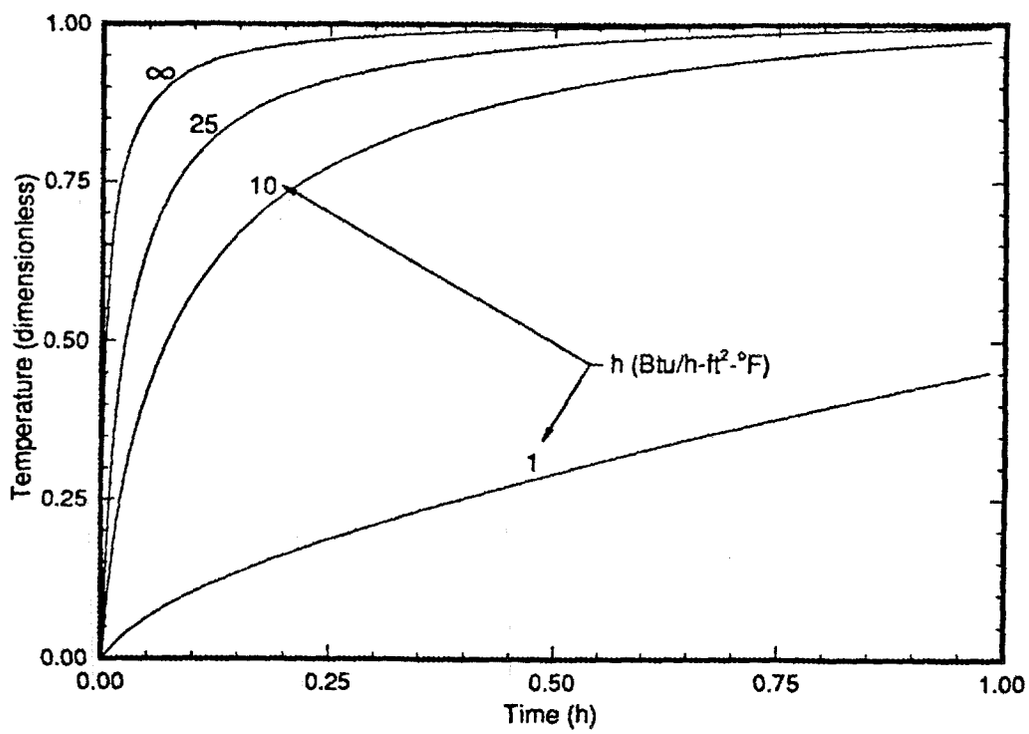

Figure 9. Results from finite difference analysis of Model 1 for varying external heat transfer coefficients.

The differences between this assumed heat transfer coefficient and infinite heat transfer (i.e., the skin of the Gator is equal to the environmental temperature) disappear after the first hour. Since few missions take less than one hour, these differences were considered inconsequential, and the value of 56.8 W/m²-°C (10 Btu/h-ft²-°F) can be used with confidence for all external in-flight applications.

Natural convection conditions, such as would occur in a bomb bay enclosure, are represented by a heat transfer coefficient of 5.68 W/m²-°C (1 Btu/h-ft²-°F). The response of the mine under such sheltered conditions is much slower, as was also shown by the results from later models.

The second computer model was three-dimensional and was also run with the HEATING 7.1 finite difference computer code. The temperature-vs-time plots for three potential capacitor locations of a mine in Row H are shown in Fig. 10. The three locations are the 0°, 45°, and 90° azimuthal positions in the model. The 0° position corresponds to the mine being rotated so that the capacitor location is below the location of minimum polyurethane dunnage thickness. The 90° position corresponds to the mine being

rotated so that the capacitor location is below the location of maximum polyurethane dunnage thickness. There are actually three curves on Fig. 10, but they are so close together that they are hard to distinguish. These surface temperatures and other results from the Model 2 analysis show that there is very little azimuthal temperature variation within the mine.

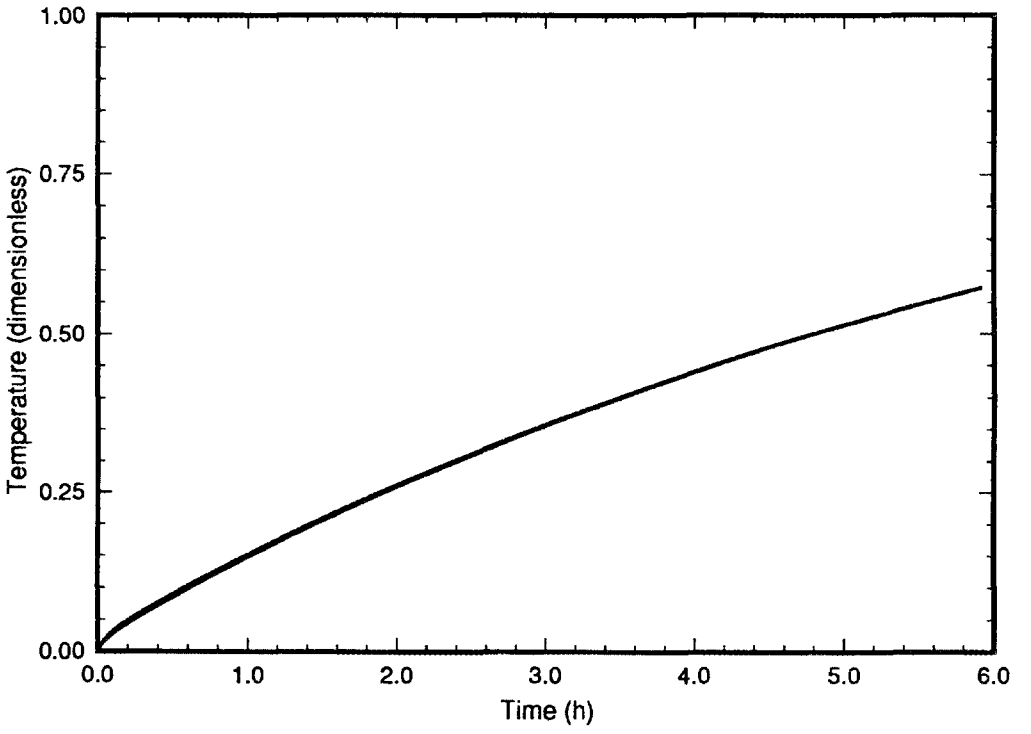

Figure 10. Results from finite difference analysis of Model 2 for three angular positions of mine in Row H.

Both Models 1 and 2 included only a half-height of the mine (compare Fig. 7 to Fig. 1). However, unlike Model 1 which looked at a single mine directly exposed to the environment, the midplane (height = 0.0 in Fig. 7) of the mine in Model 2 is not an approximate plane of thermal symmetry. The other half of the mine, as well as the other mines in the assembly, represent additional thermal mass which is not included in the model, and this additional thermal mass is more isolated from the exterior environment that the portion modeled. This means that in reality the mine will respond less rapidly to the step change in environmental temperature than the model predicts (i.e., the model is conservative). The fact that the temperature within the mine is fairly uniform throughout the transient indicates that the detailed model of the mine itself is not necessary. Therefore the second model was not extended to include the entire mine.

Model 3 used a simpler representation of the mine, but a much more complete representation of the Gator components surrounding the mines. This was done to explore more fully the issues of mine placement (particularly with respect to the aluminum strongback), uncertain dunnage conductivity, and variable external heat transfer coefficient. This finite element analysis was described in Sect. 4.1 and permits a more accurate representation of the irregular shapes making up the Gator system. Figures 11 and 12 show that the three most exposed mine locations have very similar temperature responses. The differences are slightly modified when the dunnage conductivity is increased, as can be seen by comparing

Figs. 11 and 12. With the lower dunnage conductivity of Fig. 11, the mines near the aluminum strongback in Row F show the quickest temperature change. When the dunnage conductivity is increased in Fig. 12, the mine nearest the thinner dunnage location, in Row H, shows the quickest thermal response. Based on the information available, the Gator dunnage conductivity should be between these two values. However, the differences are so slight that the general conclusion of this examination must be that the three mine locations considered generate essentially identical mine temperatures. The uncertainty associated with the dunnage conductivity also makes very little difference in the final temperature profiles. Row D is completely unaffected, and the other two locations are changed by less than 5% over a 14-h period.

The results shown in Figs. 11 and 12 were applied to a specific mission profile with an initial temperature of 15.6°C (60°F), an ambient cruising temperature of -62°C (-80°F), and a flight speed of Mach 0.77 (giving a recovery temperature of -40°F at an assumed recovery factor of 0.89). The process of transforming the step temperature change data to mission-specific data is described in Sect. 6. The results for this mission specification are shown in Figs. 13 and 14. Here, the uncertainty associated with the dunnage conductivity results in a variation in the minimum mine temperature of only 2°C (4°F), from -27 to -29°C (-17 to -21°F), after a 12 hour flight duration. The difference is less for shorter flights. This uncertainty is well within the bounds of uncertainty associated with any computer model of a physical process.

To determine the effect of different external surface heat transfer coefficients, additional calculations were performed with external heat transfer coefficients of 5.7 and 568 W/m^2-°C (1 and 100 Btu/h-ft^2-°F). The results for a mine in Row H are shown in Figs. 15 and 16, and the trends are similar to those found for Model 1, previously shown in Fig. 9. Again, there is very little difference between coefficients expected for external Gator locations, between 57 and 568 W/m^2-°C (10 and 100 Btu/hr-ft^2-°F). And the large difference between internally-housed Gators exposed only to natural

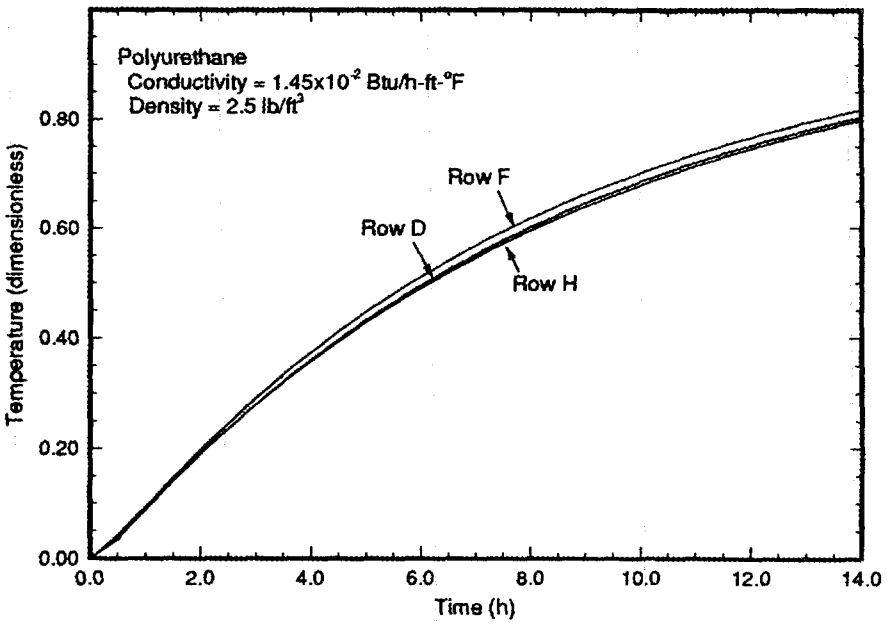

Figure 11. Results from finite element analysis of Model 3 with low-conductivity polyurethane for three mine locations.

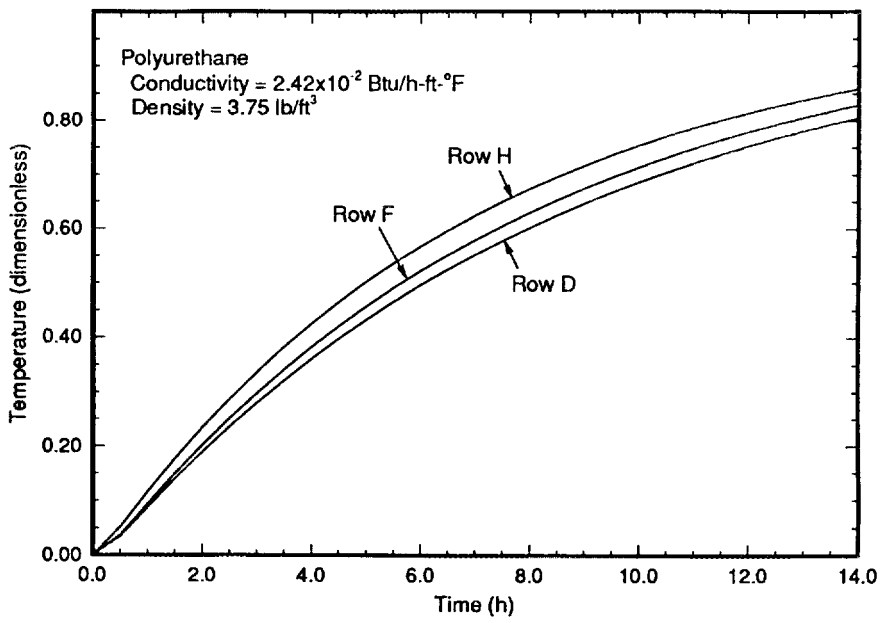

Figure 12. Results from finite element anlysis of Model 3 with high-conductivity polyurethane for three mine locations.

convection and those hung outside the plane is again shown clearly. These figures also show the combined effect of changes in external heat transfer coefficient and variations in dunnage conductivity for the mine location most affected by these variations.

The results from Model 2 for Row H shown in Fig. 10 were utilized to develop Eq. 10 that expresses internal temperature in terms of initial and recovery temperatures and the time following the step change in external temperature. Using Eq. 10, the Model 2 results were then extrapolated and applied to the same mission profile described above [15.6°C (60°F) initial and -40°C (-40°F) recovery temperatures] for Model 3. The results for these two models are compared in Fig. 17. The slight difference between the results for Models 2 and 3 is mostly caused by the different ways of modeling the polyurethane dunnage. The dunnage is modeled quite explicity in Model 3, compared to the much cruder dunnage approximation of Model 2. A secondary contributer to the difference between the results would be the lumped capacitance mine treatment in Model 3. That is, the TOPAZ results reflect an average mine temperature while the HEATING 7 results reflect a point near the mine surface. Also, as discussed previously, the HEATING 7 results are somewhat conservative in that they account for only half of the mine's thermal capacitance and none of the surrounding mines. Given these differences in the models, the agreement between the results is quite extraordinary. Note that the polyurethane conductivity is expected to lie between the Lo-K and Hi-K curves shown on this figure.

$$T = T_i + (T_r - T_i)(1 - 0.9841e^{-0.142194\tau}) \tag{10}$$

where:

T = temperature of mine in Row H at time τ, °F,
T_i = initial temperature of Gator system, °F,

T_r = recovery temperature, °F, and
τ = time, h.

5.2 Hand Calculations

Just as for the computer model, a normalized step temperature change was used for the hand calculations. The results for a time 8 h after the step change in temperature are summarized in Table 5 where T_n^* is defined by Eq. 7 and T_n is defined by Eq. 6. All cases represent a location near the surface of the Gator weapon protected by a minimal thickness of polyurethane dunnage except for the last case where it is noted that it represents a position near the thinnest section of the aluminum strongback.

The results clearly show the effect of the assumed composite conductivity and the Gator shell structure. As discussed previously, the internal structure of the Gator is such that selection of a single homogeneous conductivity is anything but straightforward. The steel casings surrounding each mine have relatively high conductivities while the plastic aerodynamic housings that surround each mine are good insulators. If a higher conductivity is assumed, the heat capacity of all the mines is available to absorb an abrupt temperature change and therefore slow down temperature changes near the surface of the missile. Note that for this mass-average case the axis and surface temperatures are equal after the 8 h period. If the lowest conductivity is used, the mines near the surface lose most of their heat to the environment without the buffering effect of the rest of the mass within the Gator missile. Note that for the lowest conductivity case, the surface temperature is very close to the environmental temperature while the axis temperature is still very near the initial Gator temperature. Relatively small temperature differences between mines in the center of the Gator and mines near the surface can be seen in the volume-average case. This case also shows the slowest response of the internal Gator components near the surface, reaching only 63% of the temperature step after 8 h. The high insulation value of the

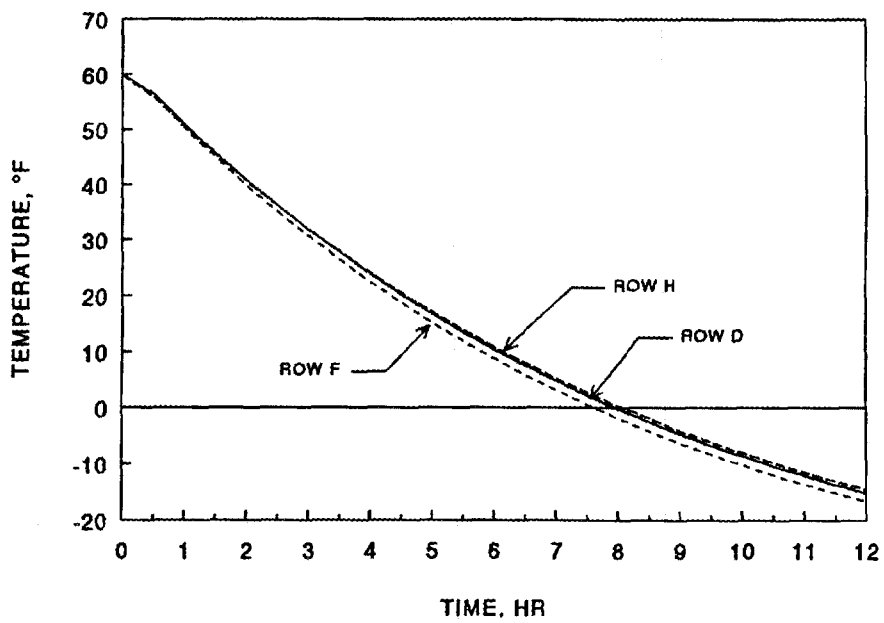

Figure 13. Model 3 results for low-conductivity (0.0145 Btu/h-ft-°F) polyurethane applied to mission with 60°F initial and -40°F recovery temperatures.

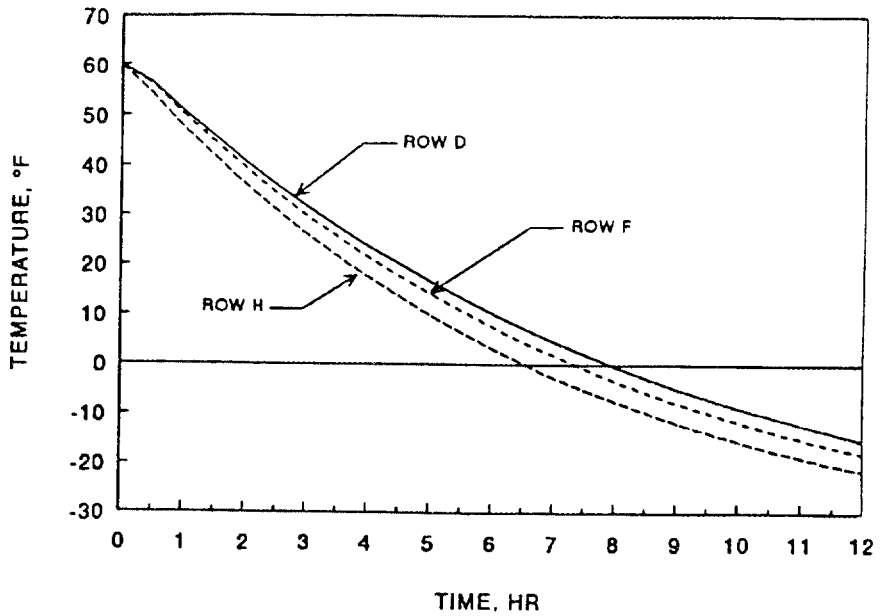

Figure 14. Model 3 results for high-conductivity (0.0242 Btu/h-ft-°F) polyurethane applied to mission with 60°F initial and -40°F recovery temperatures.

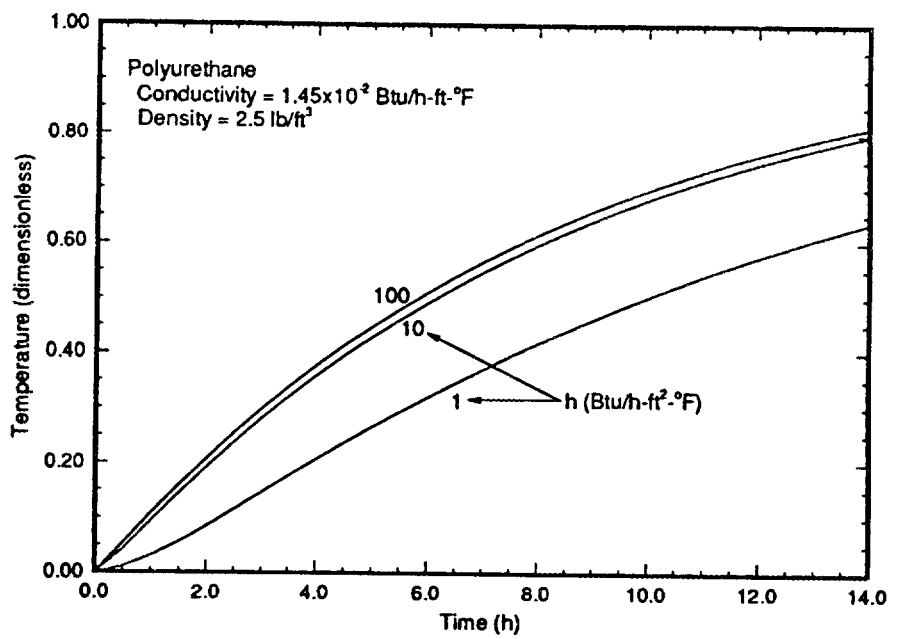

Figure 15. Results from finite element anlysis for Row H mine in Model 3 with low-conductivity polyurethane for three external heat transfer coefficients.

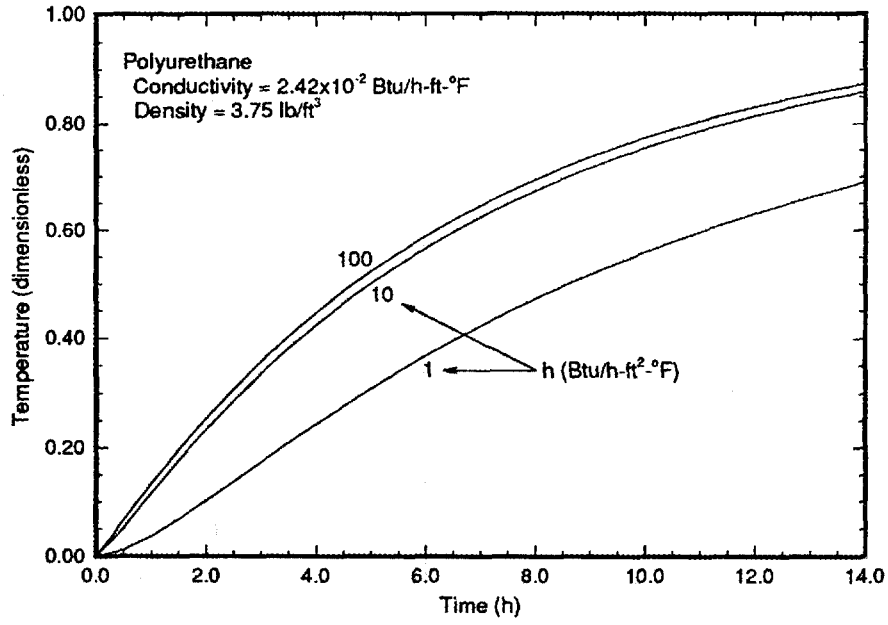

Figure 16. Results from finite element analysis of Row H in Model 3 with high-conductivity polyurethane for three external heat transfer coefficients.

polyurethane dunnage is shown best by comparing the mine temperatures near the aluminum strongback to those near the minimum level of insulation. Here the simplified model predicts that enhanced heat transfer will bring the Gator internals to 92% of the temperature step after only 8 h.

Table 5. Gator temperature estimates 8 h after step change in environmental temperature

Conductivity	Biot Number	Fourier Number	T_n^* (axis)	T_n^* (r/R=1.0)	T_n (r/R=1.0)
Mass-average	0.03	22.	0.27	0.27	0.73
Lowest	4.2	0.15	0.82	0.23	0.77
Eucken volume average	0.4	1.25	0.44	0.37	0.63
Eucken volume average, near aluminum strongback	1.14	1.25	0.14	0.08	0.92

These hand calculations were performed to verify the reasonableness (within an order of magnitude) of the computer models. The first two computer models evaluated a portion of a mine located within the Gator system near the surface at a point of minimum dunnage thickness. The surface of the

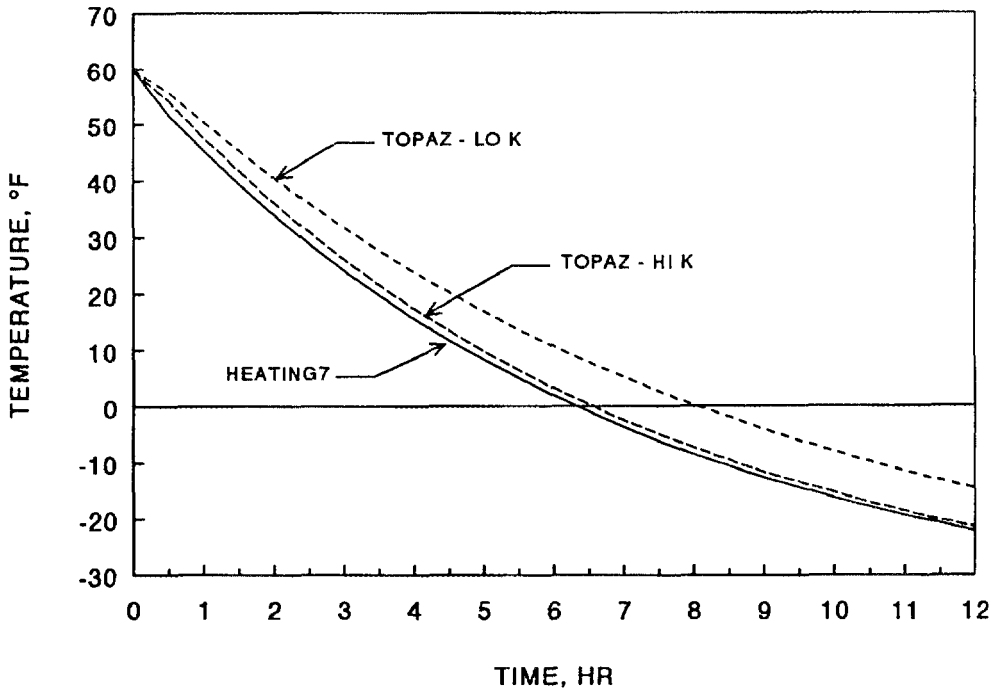

Figure 17. Comparison of Model 2 (HEATING 7) and Model 3 (TOPAZ) results for Row H mine during a mission with 60°F initial and -40°F recovery temperatures.

mine facing away from the Gator surface was assumed to be adiabatic. These assumptions were chosen to represent the worst case (i.e., the case where the mine component would face the most exposure to the cold outdoor temperatures). Under these assumptions, the predicted dimensionless temperature after 8 h was ~0.6 for both Models 2 and 3, as shown in Figs. 11 and 12. This result is most closely comparable to the assumption of low conductivity with minimum dunnage, where the estimated dimensionless surface temperature after 8 h was 0.63. The worst disagreement between this simplified model and the detailed computer model is for the region near the aluminum strongback. Here the simplified model predicts much colder temperatures than the computer model, although still within the order of magnitude accuracy expected. The difference can be understood by noting that the simpler model conservatively assumes a constant aluminum thickness equal to the smallest aluminum thickness and gives no credit for the buffering air spaces. Both the variation in aluminum thickness and the air spaces can be seen clearly in Fig. 4. Considering this difference between the two models, the results differ in the expected direction and within a reasonable magnitude.

Given the limited nature of the homogeneous model, the difference of only 5% for the one case is exceptional. Both models agree that the thermal response to external temperature changes is relatively slow within the Gator system, even under the most conservative of assumptions. Overall, the hand calculations confirmed that the finite difference computer model has produced reasonable results, as expected.

6. MISSION APPLICATIONS

The ultimate goal of this analysis is to determine whether the possibility exists that a failure condition would be encountered within the mission profile envelope. It is important to correctly apply the analysis results to Gator mission profiles to identify such potential failures. However, Gator mission profiles are not clearly defined and may be modified for future use. Therefore, the analysis has been done in such a way as to permit the results to predict internal temperatures for almost any scenario.

All analyses were performed for a step temperature change, and the analysis results were presented in Sect. 5 for a normalized step magnitude of 1. These results can be applied to any mission profile to determine the minimum mine temperature. This requires knowledge of both the initial temperature and the coldest recovery temperature. (Recovery temperature should be calculated as discussed in detail in Sect. 3). The results can be applied for either externally hung systems, or systems carried within bomb bays. This section provides graphs helpful in applying the results to specific missions and several examples.

6.1 Mission Temperature Profile

The environmental temperature for the Gator changes as the plane takes off, climbs to cruising altitude, travels to its destination, and then descends and drops the missile. The analysis results in Sect. 5 clearly show that any trip with a total travel time less than ~5 h will not cause mine temperatures to drop below the limiting minimum temperature of -31.7°C (-25°F). Therefore the temperature variations during the initial climb are not of concern. Also, the temperature variations during the projectile's descent will tend to warm, not cool, the mines and are not of concern. The coldest environmental temperature experienced by the Gator system, usually the cruising altitude temperature, should therefore be used.

For externally mounted Gators, this environmental temperature must be corrected by the recovery factor discussed in Sect. 3. Figure 18 shows the recovery temperature as a function of ambient temperature, cruising speed, and recovery factor. For Gators carried in bomb bays, the lowest temperature expected in that enclosure should be used.

For conservatism, the total mission time should be used in all calculations.

6.2 Applying Normalized Step Temperature Data

The results presented in Sect. 5 show the normalized temperature variation as the time varies from 0 to 14 hours. The application of these results to actual missions is shown in Eq. 11.

$$T_{gi} = T_i - [T_n \times (T_i - T_r)] \tag{11}$$

where:

T_{gi} = internal Gator temperature,
T_i = initial temperature,
T_n = normalized temperature from this analysis, and
T_r = recovery temperature.

For example, assume a mission is expected to take 6 h with an initial temperature of 27°C (80°F) and a minimum recovery temperature of -34°C (-30°F). Looking at Fig. 10 in Sect. 5, the internal normalized temperature is 0.57 after 6 h. Using Eq. 11, the mine temperature can be expected to drop to ~-8°C (17°F). Another way of examining this example is to look at Fig. 19. From this figure, it can be seen that for an initial temperature of 27°C (80°F) and a recovery temperature of -34°C (-30°F), the mine will

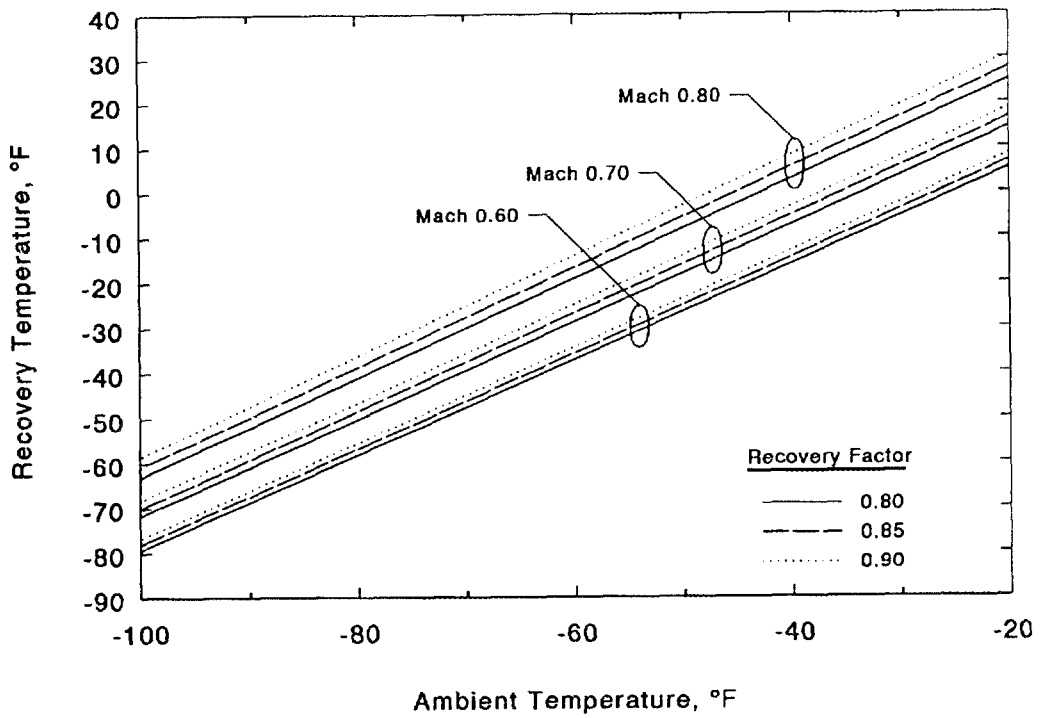

Figure 18. Effects of ambient temperaure, Mach number, and recovery factor on recovery temperature.

not reach the minimum limiting temperature of -31.7°C (-25°F) until sometime after 14 h, so a 6 h mission should pose no problem.

Figure 19 was developed from the results of the second model using Eq. 10 and shown in Fig. 10, and provides general guidance on the longest possible mission for any combination of initial and recovery temperatures. Considering the degree of conservatism embodied in this analysis, any mission with a total length shorter than the exposure duration shown on this figure should safely maintain the mines at a temperature at or above -31.7°C (-25°F).

As another example, consider a mission with a 10 h length, an initial temperature of 15.6°C (60°F), and an expected minimum recovery temperature of -51°C (-60°F). Figure 19 shows that after about 8.5 h, the mines will drop to a temperature less than -31.7°C (-25°F), and the timer circuitry could malfunction. Therefore, within this mission profile, the possibility for the cold temperature failure scenario exists.

If the Gator is carried in a bomb bay, Fig. 20 can be used to estimate the maximum mission duration. The exposure temperature shown on this figure refers to the Gator exposure, that is the internal bomb bay temperature. This figure shows that the capacitor temperature limitation will not be exceeded for missions less than ~13 h, even for the most extreme cold temperatures. As an example, assume the Gator is placed in a bomb bay, with an expected minimum temperature of -46°C (-50°F) for this 10 h

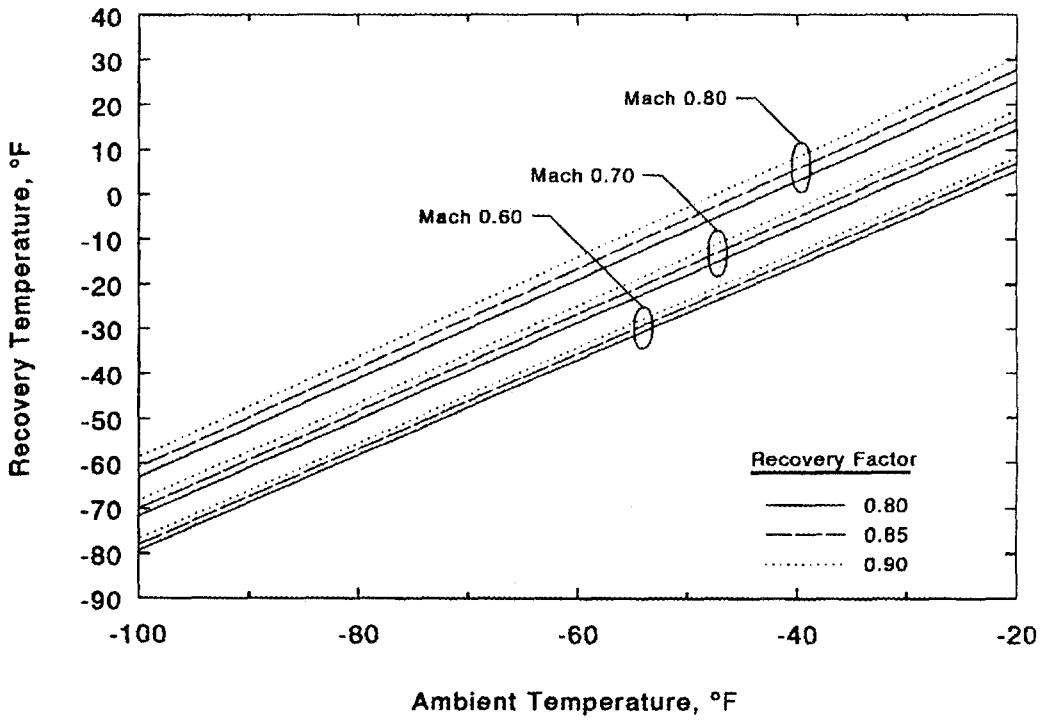

Figure 18. Effects of ambient temperaure, Mach number, and recovery factor on recovery temperature.

not reach the minimum limiting temperature of -31.7°C (-25°F) until sometime after 14 h, so a 6 h mission should pose no problem.

Figure 19 was developed from the results of the second model using Eq. 10 and shown in Fig. 10, and provides general guidance on the longest possible mission for any combination of initial and recovery temperatures. Considering the degree of conservatism embodied in this analysis, any mission with a total length shorter than the exposure duration shown on this figure should safely maintain the mines at a temperature at or above -31.7°C (-25°F).

As another example, consider a mission with a 10 h length, an initial temperature of 15.6°C (60°F), and an expected minimum recovery temperature of -15.6°C (60°F). Figure 19 shows that after about 8.5 h, the mines will drop to a temperature less than -31.7°C (-25°F), and the timer circuitry could malfunction. Therefore, within this mission profile, the possibility for the cold temperature failure scenario exists.

If the Gator is carried in a bomb bay, Fig. 20 can be used to estimate the maximum mission duration. The exposure temperature shown on this figure refers to the Gator exposure, that is the internal bomb bay temperature. This figure shows that the capacitor temperature limitation will not be exceeded for missions less than ~13 h, even for the most extreme cold temperatures. As an example, assume the Gator is placed in a bomb bay, with an expected minimum temperature of -46°C (-50°F) for this 10 h

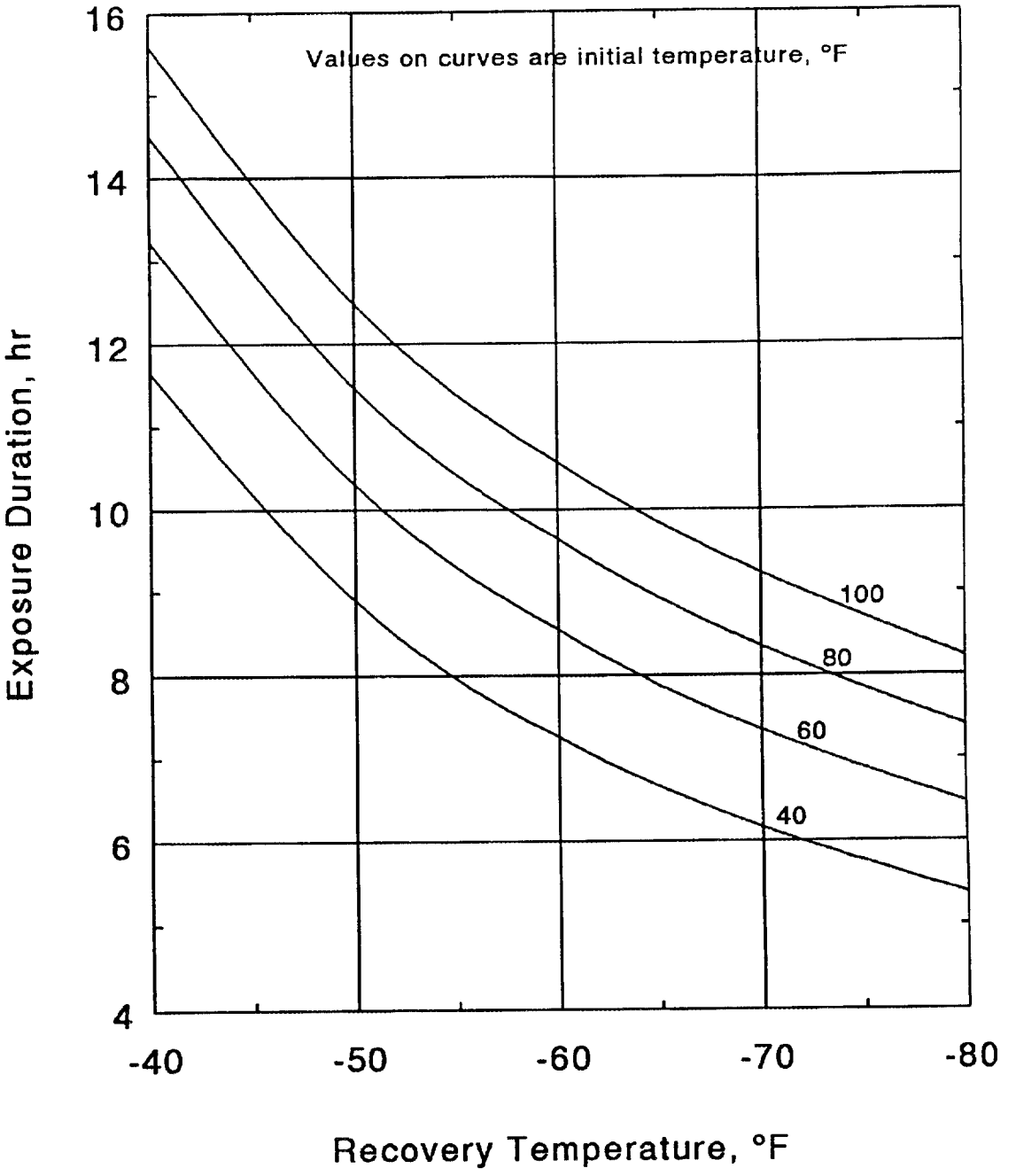

Figure 19. Predicted external exposure duration at which internal mine temperature drops to -25°F, based on results from Model 2.

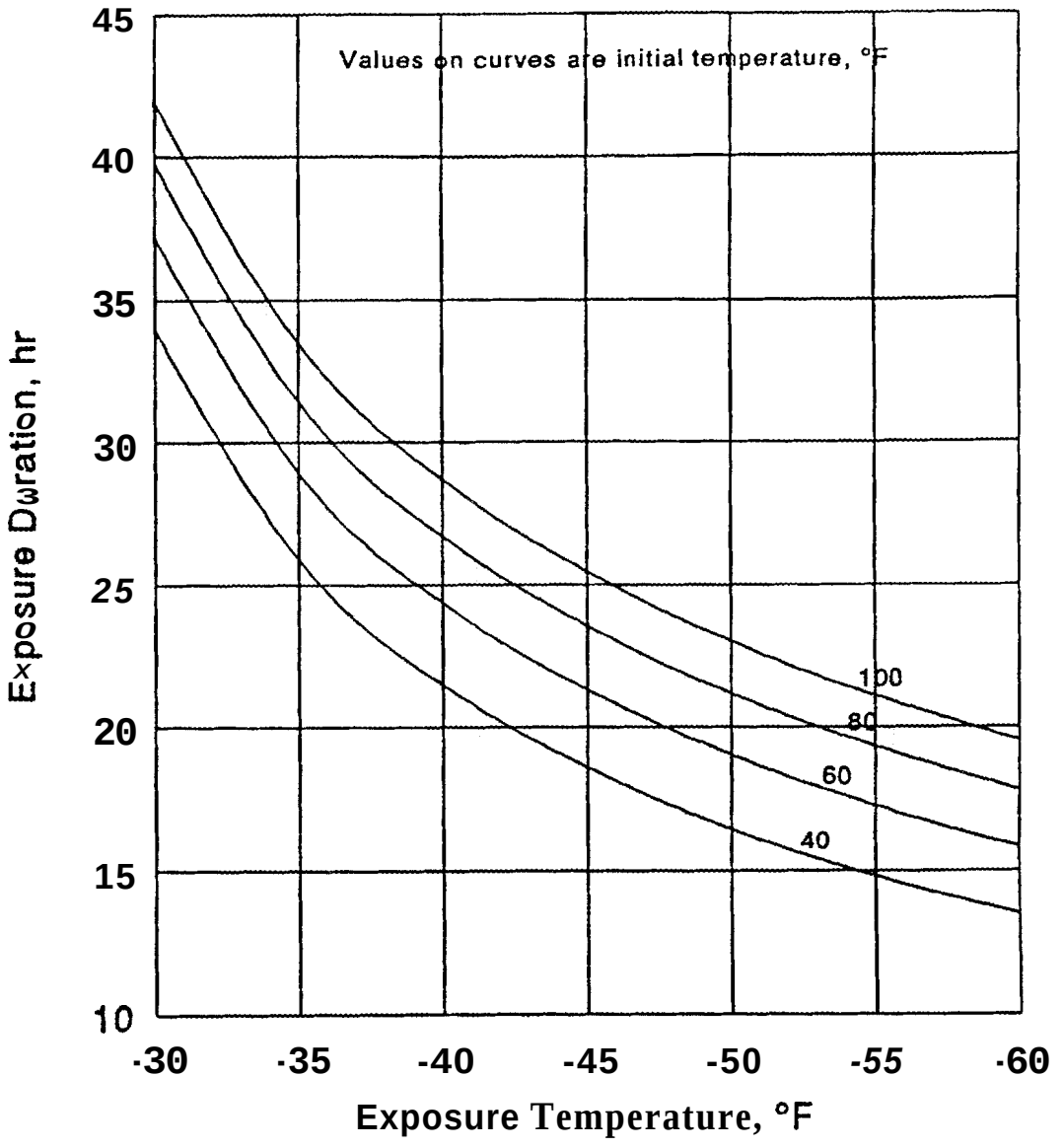

Figure 20. predicted bomb bay exposure duration at which internal mine temperature drops to - 25°F, based on results from Model 2.

mission. From Fig. 20, the safe exposure duration would be about 17 h, so the 10 h mission would pose no problem. Another way to examine this mission is to use the curve shown in Fig. 15, with an external heat transfer coefficient of 5.7 W/m^2-°C (1 Btu/h-ft^2-°F). From this figure, the normalized temperature after 10 h is ~ 0.50. Using Eq. 11, this gives a mine temperature of -15°C (5°F), well above the desired minimum of -31.7°C (-25°F).

7. CONCLUSIONS

The goal of this analysis has been to identify the mission profile envelope where the cold temperature failure scenario may be encountered. The analysis used several approaches to identify the coldest internal location and the thermal response of that location. Efforts also focussed on quantifying the impact of several uncertainties, including unknown material properties and variable flight parameters. Results have been presented in a manner designed to facilitate their application to a wide range of potential mission profiles. The Gator was found to operate within reasonable temperature bounds for all short (< 5 h) flights. For longer flights, the Gator's internal temperature will depend on the external temperature, the flight speed, and the flight duration.

The authors of this analysis have used conservative assumptions wherever possible and have a high level of confidence in the results. However, experimental results are unavailable to confirm these temperature estimates. If the opportunity for such an experimental measurement becomes available, it should be used to verify and enhance the model results.

REFERENCES

1. Military Standard, *Climatic Information to Determine Design and Test Requirements for Military Systems and Equipment*, MIL-STD-210C, 9 January 1987, AMSC F2302.

2. MIL-STD-1670A

3. *U.S. Standard Atmosphere, 1976*, National Oceanic and Atmospheric Administration, National Aeronautics and Space Administration, and United States Air Force, October 1976, Washington, D.C.

4. S. L. Valley, ed., *Handbook of Geophysics and Space Environments*, U.S. Air Force Cambridge Research Laboratories, McGraw-Hill, 1965.

5. W. H. McAdams, *Heat Transmission*, Third Edition, McGraw-Hill, 1954.

6. J. P. Cullen and E. Gilliam, *Aerodynamic Cooling of the B-52 Carried Quickstrike Mine Mark 65 Mod 1*, NSWC TR 88-10, Naval Surface Warfare Center, Dahlgren, VA, 1988.

7. K. W. Childs, ***Heating 7.1 User's Manual***, K/CSD/TM-96, Oak Ridge National Laboratory, Oak Ridge, TN, July 1991.

8. A.B. Shapiro, TOPAZ-2D - A Two-dimensional Finite Element Code for Heat Transfer Analysis, Electrostatics, and Magnetostatics Problems, UCID-20824, Lawrence Livermore National Laboratory, Livermore, CA, July 1986

9. V. S. Arpaci, Conduction Heat Transfer, Addison-Wesley Publishing Company, Reading, MA, 1966

10. A. Eucken, Ceram. Abstr. 11 (11), p. 576, 1932

11. ASHRAE Handbook, 1989 Fundamentals, American Society of Heating, Refrigerating, and Air Conditioning Engineers, Inc., Atlanta, GA, 1989

12. Frank Kreith, Principles of Heat Transfer, 3rd Edition, Intext Educational Publishers, New York, NY, 1973

13. J. H. Perry, Chemical Engineers' Handbook, 4th Edition, McGraw-Hill Book Company, New York, NY, 1963

DISTRIBUTION LIST FOR GATOR REPORT (ORNL/TM-12274)

Internal Distribution

1. M. Ammons
2. D. Bopp
3. D. A. Casada
4. K. W. Childs
5. H. Clift
6. W. G. Craddick
7. R. M. Davis
8. J. Dillon
9. E. C. Fox
10. W. Griest
11. J. Hanna
12. J. E. Jones Jr
13. G. Keck
14. D. Lloyd
15. D. Mee
16. D. G. Morris
17. J. C. Moyers
18. M. Olszewski
19. D. Robinson
20-25. T. K. Stovall
26. K. Vandergriff
27. J. Walls
28. ORNL Patent Office
29. Central Research Library
30. Document Reference Section
31. Laboratory Records Department
32. Laboratory Records (RC)

External Distribution

33. Tom Brown, General Engineer, Picatinny Arsenal, New Jerey, 07806-5000
34-56. Paul E. Chiodo, Acting Chief, Nuclear Systems and Stockpile Reliability Division, SMCAR-QAN, Picatinny Arsenal, NJ 07806-5000
57. Robert J. Kuper, Chief, Packaging Division, SMCAR-AEP, Picatinny Arsenal, NJ 07806-5000
58. Gary Adler, Chemical Engineer, SMCAR-QAN, Picatinny Arsenal, NJ 07806-5000
59. Michael Cassiello, Project Leader, Pred. Tech. Branch, SMCAR-QAN, Picatinny Arsenal, NJ 07806-5000
60. Jack Kevorkian, Chief, Pred. Tech. Branch, Picatinny Arsenal, NJ 07806-5000
61. Ed Persau, Acting Branch Chief, Test & Reliability, SMCAR-QAN, Picatinny Arsenal, NJ 07806-5000
62. Mitch Primas, General Engineer, Picatinny Arsenal, NJ 07806-5000
63. Lynn Ryder, FSAC, Picatinny Arsenal, NJ 07805-5000
64. George Tellschow, FSAC, Picatinny Arsenal, NJ 07805-5000
65. Henry Van Dyke, Acting Project Leader, Picatinny Arsenal, NJ 07805-5000
66. Assistant Manager, Energy Research and Development, U.S. Department of Energy, Oak Ridge Field Office, P.O. Box 2001, Oak Ridge, TN 37831
67. U.S. Department of Energy, Office of Scientific and Technical Information, P.O. Box 62, Oak Ridge, TN 37831